AD-A071 048 BINARY SYSTEMS INC SALIDA CO F/G 20/4
FURTHER RESULTS ON AN ARRAY DESIGN TO MEASURE THE WAVENUMBER-FR--ETC(U)
FEB 79 L W BROOKS N00014-72-C-0318
UNCLASSIFIED CBR-79-01 NL

| OF |
AD A071048

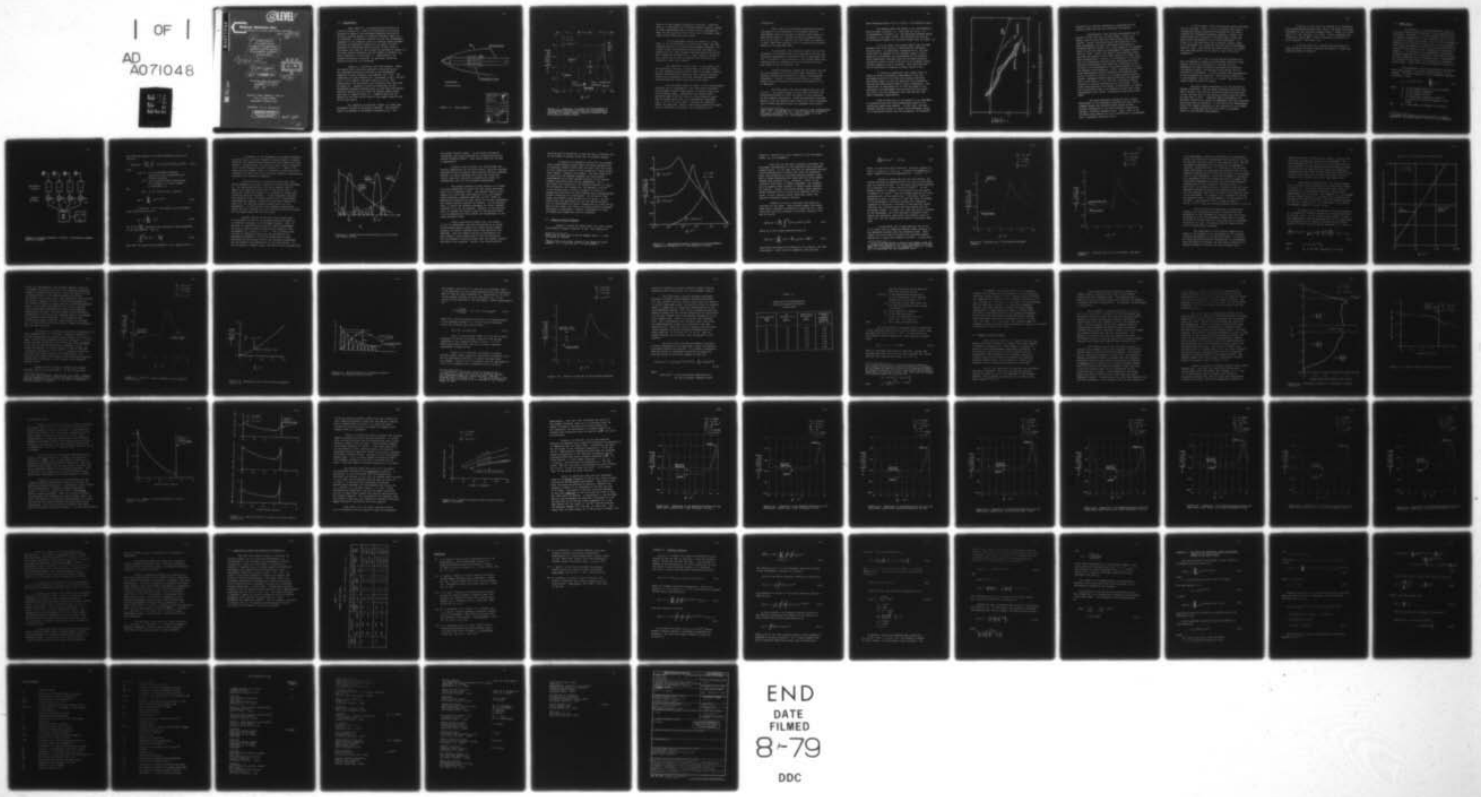

END
DATE FILMED
8-79
DDC

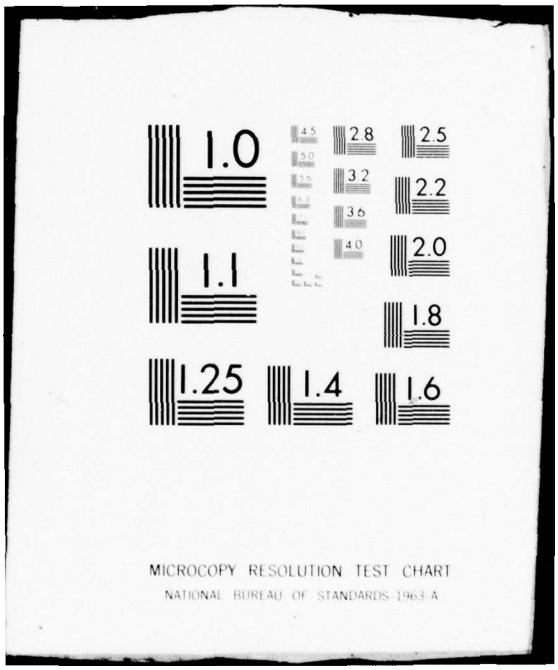
1.0
1.1
1.25
1.4
1.6
1.8
2.0
2.2
2.5
2.8
3.2
3.6
4.0
4.5
5.0
5.6
MICROCOPY RESOLUTION TEST CHART
NATIONAL BUREAU OF STANDARDS-1963-A

(12) LEVEL II

Binary Systems Inc.

303 E Street, P.O. Box 1105, Salida, CO 81201 (303) 539-3060

Report No. CBR-79-01 (14)

(6)

FURTHER RESULTS ON AN ARRAY DESIGN TO MEASURE THE WAVENUMBER-FREQUENCY SPECTRUM BENEATH AN AXISYMMETRIC TURBULENT BOUNDARY LAYER.

(9) Final rept.,

BY

(10) LOWELL W. BROOKS

(11) 5 February 1979

(12) 75p.

Performed Under ONR Contract No. N0014-72-C-0318 (15)

FOR

OFFICE OF NAVAL RESEARCH, CODE 222
800 N. QUINCY STREET
ARLINGTON, VIRGINIA 22217

ATTENTION: Mr. H. Fitzpatrick

1.0 INTRODUCTION

This report is an extension and correction of previous results [1]. Here the requirements on an array designed to measure the wavenumber-frequency spectrum of the wall pressure beneath a turbulent boundary layer will be discussed. Of specific interest will be the axisymmetric component of the pressure field on a axially towed cylinder. The basic configuration consists of an array of flush-mounted ring transducers where the axis of the array is coincident with that of the cylinder as sketched in Figure 1.1. The major design parameters are the number of elements, N_e, their separation, d, and width, w. Additionally, the channel-to-channel tolerances on amplitude, phase and spacing errors will be considered.

Figure 1.2 illustrates the basic problem. There, two models which have been proposed to describe $P_o(k,\omega)$, the wavenumber-frequency spectrum of the axisymmetric component of wall pressure, are compared ([2], [3]). The comparison has been computed for a frequency of $\frac{\omega}{2\pi} = 100 \text{ sec}^{-1}$ and a 3 inch diameter cylinder towed at 15 kts. The normalization for the spectra are consistent with that used by Chase [2]. Appendix A gives the definition of the wavenumber-frequency spectrum which is used here and details explicit formulas for the Chase and Gardner models which were used to compute Figure 1.2. Symbols which are not defined in the text can be found in the symbol table at the end of this report.

For numerical orientation, Figure 1.2 shows some wavenumber regions of particular interest. The acoustic region corresponds to wavenumbers bounded by $|k| < \omega/c$

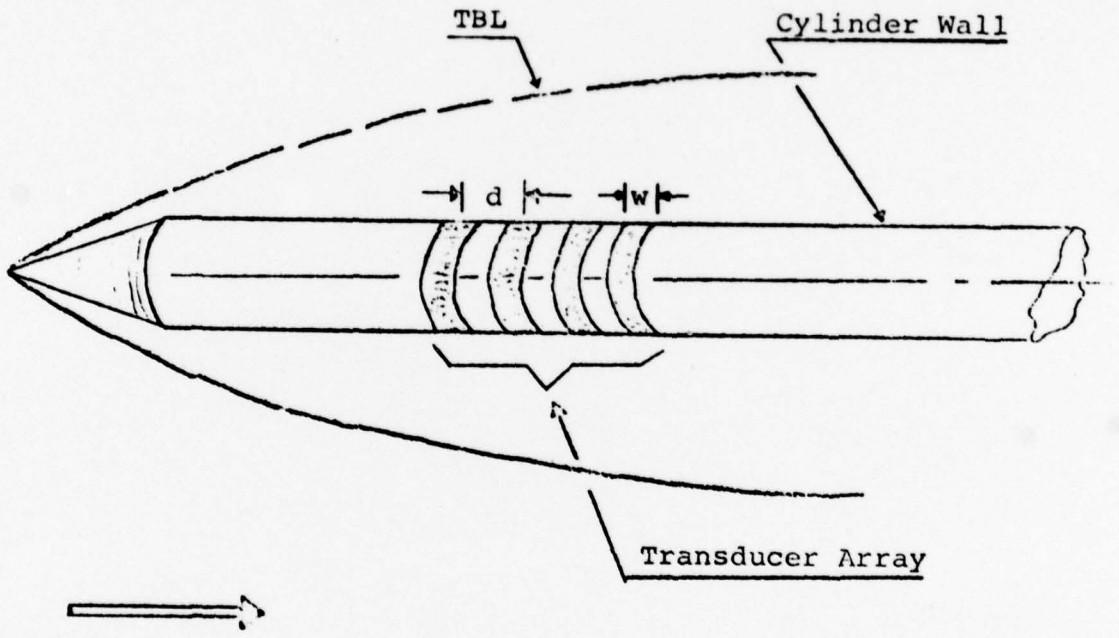

Figure 1.1. Array Geometry.

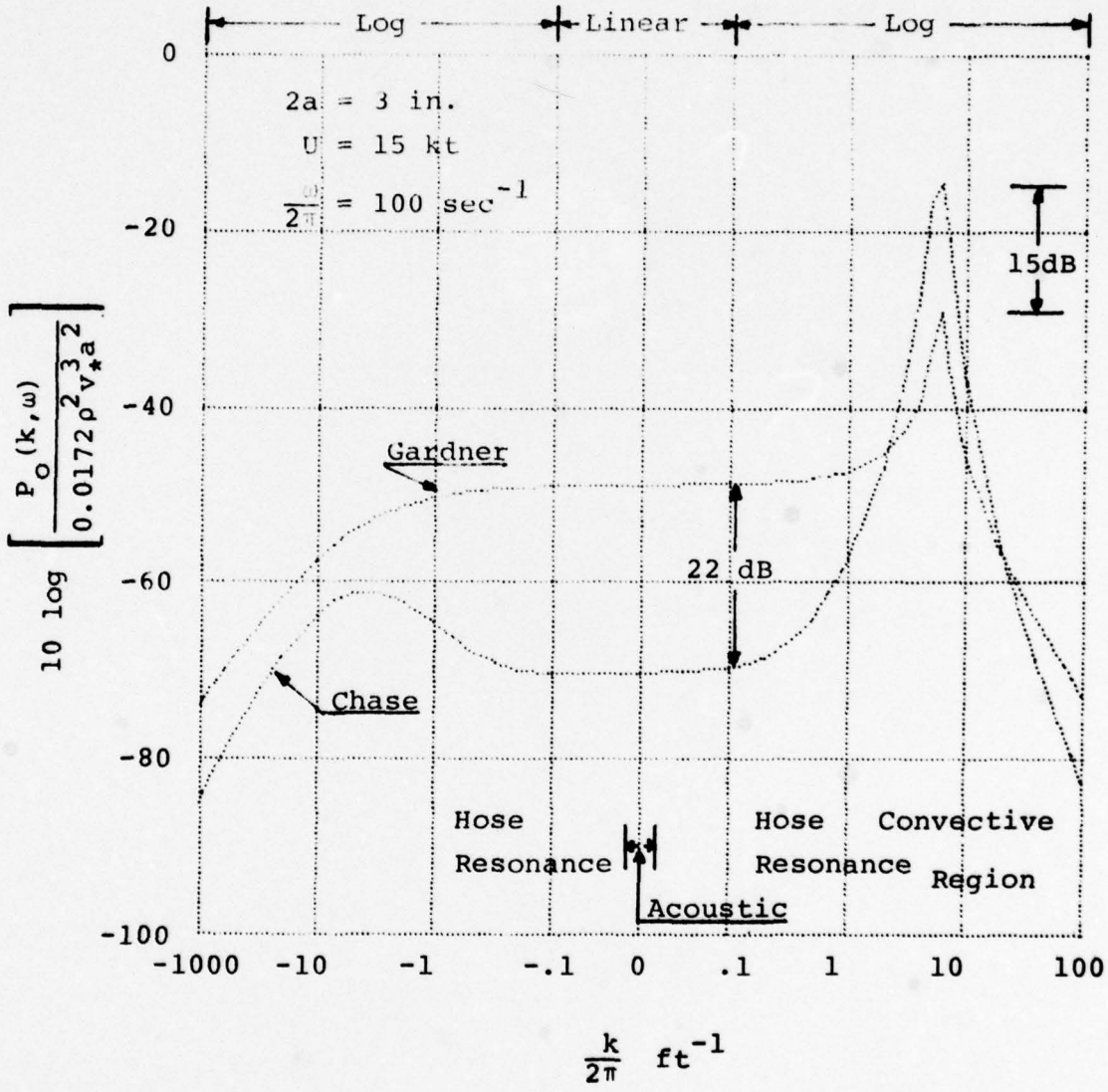

Figure 1.2. Comparison of Gardner and Chase Models of the Wavenumber-Frequency Spectrum for the Axisymmetric Component of Pressure under a Turbulent Boundary Layer on an Axially Towed Cylinder.

where c is the acoustic propagation velocity. Since the goal of a towed array is to detect acoustic signals, energy at these wavenumbers must be passed with no attenuation. Thus, the TBL spectral level here places an ultimate lower bound on the towed array self noise.

In the wavenumber region for which $|k| \simeq \omega/c_o$, where c_o is the breathing (or bulge) wave speed, the hose transfer function of a towed array reaches a maximum. For a small group of hydrophones located near the axis of a towed array, the hose transfer function governs the direct TBL contributed pressure level. Thus, spectral levels in this region can be used to estimate self noise for low scattering towed array modules.

The convective region near $k = \omega/U_c$, where U_c is the convection velocity, contains most of the TBL energy. At hose impedance discontinuities such as endcaps, internal spacers, hydrophones or telemetry cans, energy from this region can be scattered into hose resonance wavenumbers and significantly affect towed array self noise.

The two models shown on Figure 1.2 are significantly different at all wavenumbers. The Chase model indicates a low wavenumber content approximately 22 dB less than that of the Gardner model. Conversely, the Gardner model indicates some 15 dB less energy at the convective peak. The two models cross over at an intermediate wavenumber ($\frac{k}{2\pi} \simeq 2.2$ ft^{-1} in this case). Although the numerical values are different, similar differences between the models occur at different tow speeds, array diameters, and

frequencies.*

Since there are significant differences between the models, it is reasonable to ask whether existing experimental data can be used to indicate which model is more nearly correct. Although a detailed demonstration will not be given, it appears that the answer is negative. In fact, each model appears to fit a selected but different subset of the available data.

In particular, the numerical values for the free parameters in the Chase model were obtained by fitting the laboratory experiments of Willmarth and his associates [4], [5]. In contrast, the parameters in the Gardner model were evaluated using a combination of the Willmarth data and data taken at sea by Markowitz [6].

A major difference between the laboratory and the sea tests appears in the frequency power spectrum of the pressure fluctuations measured by a small, flush-mounted transducer. Figure 1.3 compares the Chase or Gardner models with this spectrum as measured by Willmarth et.al. or Markowitz.

The Chase model fits the Willmarth data well for $\omega a/U \gtrsim 6$. For larger values of $\omega a/U$ Chase attributes the differences between the data and model to area averaging by the pressure transducers. Chase has developed alternate models to fit the Markowitz data which will not be discussed here as Chase apparently does not recommend those models.

---

*Both models (as used here) can be written in the dimensionless form -- $P_o = \rho^2 v_*^3 a^2 f(\frac{\omega a}{U}, ka)$; thus the important parameters for model comparisons are the Strouhal number, $\omega a/U$ and normalized wavenumber, ka. (See Appendix A)

Area averaging should not be a factor in the Markowitz data.

The Gardner model was chosen to fit the Markowitz data as shown in Figure 1.3. Note that for $\omega a/U = 3.0$ (corresponding to Figure 1.2), the difference between models on Figure 1.3 is about 10 dB. This accounts for much of the difference between the convective peaks seen in Figure 1.2.

It is not clear (for either model) that the same parameter set will suffice to describe both laboratory and sea tests. In particular, Willmarth et.al. [4] have noted that the symmetry of the boundary layer is quite sensitive to alignment and straightness of the cylinder. Those experiments indicated that the cylinder should be straight to within a small fraction of its diameter before axially symmetric flow is obtained. This criterion may not be satisfied by flexible cylinders towed at sea.

It should be emphasized that neither model is based on direct experimental measurement of the low-wavenumber portion of the TBL wall pressure spectrum. The Gardner model is entirely empirical with parameters derived from measurements made by small transducers. The Chase model is semi-empirical in that the shape of the spectrum at low wavenumber has been derived from theory, but again, the free parameters have been derived from small transducer measurements.

Some verification of the models at low wavenumber is available from self noise measurements made on low scattering towed array modules. In this case, the hose transfer function serves to reject high wavenumber energy. If no scattering occurs near the hydrophone, the pressure

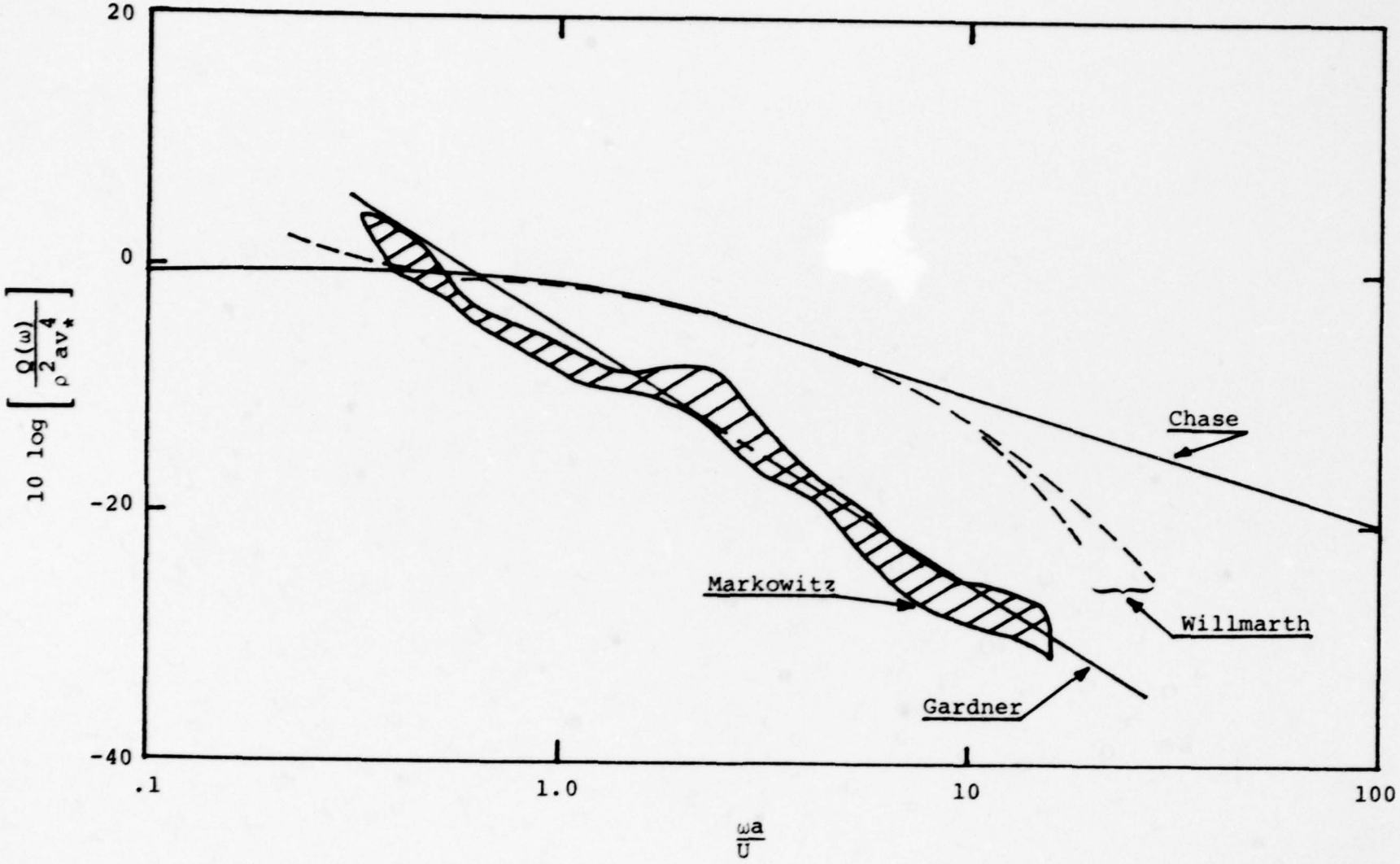

Figure 1.3. Comparison of the Chase and Gardner Models for the Point Pressure with the Experiment Measurements of Willmarth and Markowitz.

measured by an internal hydrophone is dominated by the spectral power near the hose resonance wavenumbers.

Unfortunately, such internal measurements do not provide a clear cut test of either model. First, the models tend to cross over near typical hose resonance regions. Second, relatively minor modifications in the model parameters can cause significant differences in estimated spectral levels (e.g. a 20% change in the assumed ratio of v_*/U can change the wavenumber-frequency spectral level by 3 dB). Third, the speed of the breathing waves, and thus the location of the hose resonance is often only known approximately. Fourth, it is difficult to ascertain that all significant breathing wave scattering and other sources of extraneous noise have been eliminated in the vicinity of the hydrophone so that hose resonance is truly the dominant noise mechanism. Fifth, repeatability of self noise measurements between differing tow platforms and trials is about 2-3 dB even on the same acoustic modules. Finally, agreement between model predictions and measured data on the order of 3 to 5 dB over a frequency band of interest is usually considered to be quite good. Given these uncertainities, plus others not mentioned, it should not be surprising that it is possible to find self noise measurements which "match" calculations made using either model.

The above discussion indicates that a single measurement of the wavenumber spectrum from near zero to somewhat beyond the convective peak should provide valuable information on the wall pressure fluctuations beneath a turbulent boundary layer. Thus a goal of the following array design will be to provide such a measurement over a reasonable frequency range.

In this report a very conservative design philosophy will be followed. First, it will be assumed that simple, conventional signal processing techniques will be used to estimate the wavenumber-frequency spectrum. Second, the array design will be based on the model which places the most severe requirements on the array performance. In Figure 1.2, the Chase model has a spectral dynamic range of 57 dB between the convective peak and the low-wavenumber spectral level. This range will prove difficult to measure; thus the Chase model will be used to derive the array parameters.

It is felt that the array design developed here will be adequate to measure low-wavenumber spectral levels. However, due to the stringency of the model and the assumption of simple estimation techniques for measuring the spectral levels, the resulting array design will be nontrivial to implement. It will be shown that approximately 40 array elements are required. Each element should be a 3 inch diameter ring which is 1.2 in wide. The total array length should be about 48 inches.

The most severe requirement is on the channel-to-channel tolerances. The rms phase difference should be less than 0.29 deg., the rms gain variations should be less than .06 dB, and rms error in the spacing between elements should be less than 1.7 mils. (Although these requirements are decidely nontrivial it should be remembered that they represent rms errors after calibration. In the case of the displacement errors this number represents an rms variation in the element spacing. A fixed spacing error will have a negligible impact on the spectrum measurements.)

Note that if the errors are assumed to be uniformily distributed between maximum error limits, the above rms errors correspond to the following maximum errors -- Phase: $\pm$ 0.5 deg., Gain: $\pm$ 0.1 dB, Position: $\pm$ 3.0 mils. If the tolerances are relaxed by a factor $\sqrt{2}$, a useful measurement capability is still achieved. (See Table 2.2)

A future report will consider the application of high resolution spectral estimation techniques to reduce the required number of elements.

2.0 ARRAY DESIGN

In this section, the considerations leading to the array configuration described in the introduction are discussed. Throughout, it will be assumed that the case of interest corresponds to flow along the axis of a long horizontal cylinder, and further, that only the axisymmetric component of the pressure fluctuations is to be measured. This allows the design to consist of a horizontal array of identical flush-mounted "ring" transducers as sketched in Figure 1.1. An estimate of the axisymmetric wavenumber-frequency spectrum can be obtained by filtering the output of each transducer with a narrowband filter, "beamforming" at a particular wavenumber, and averaging the resulting output power. These operations are sketched in Figure 2.1.

The beamforming operation consists of multipling the filter outputs by a weighted complex phasor V_ℓ and summing. The phasor depends on which wavenumber component is desired. Thus:

$$V_\ell = a_\ell e^{-ik_s(\ell-1)d} \; ; \qquad \sum_{\ell=1}^{N_e} |a_\ell| = 1 \tag{2.1}$$

where V_ℓ is the complex phasor on the ℓth element,
k_s is the desired wavenumber
d is the element spacing
a_ℓ is a weighting coefficient chosen to to control the sidelobe response of the array*
and N_e is the number of elements in the array.

---

* In general the weighting coefficients may be complex; however for the current design, only real a_ℓ are required.

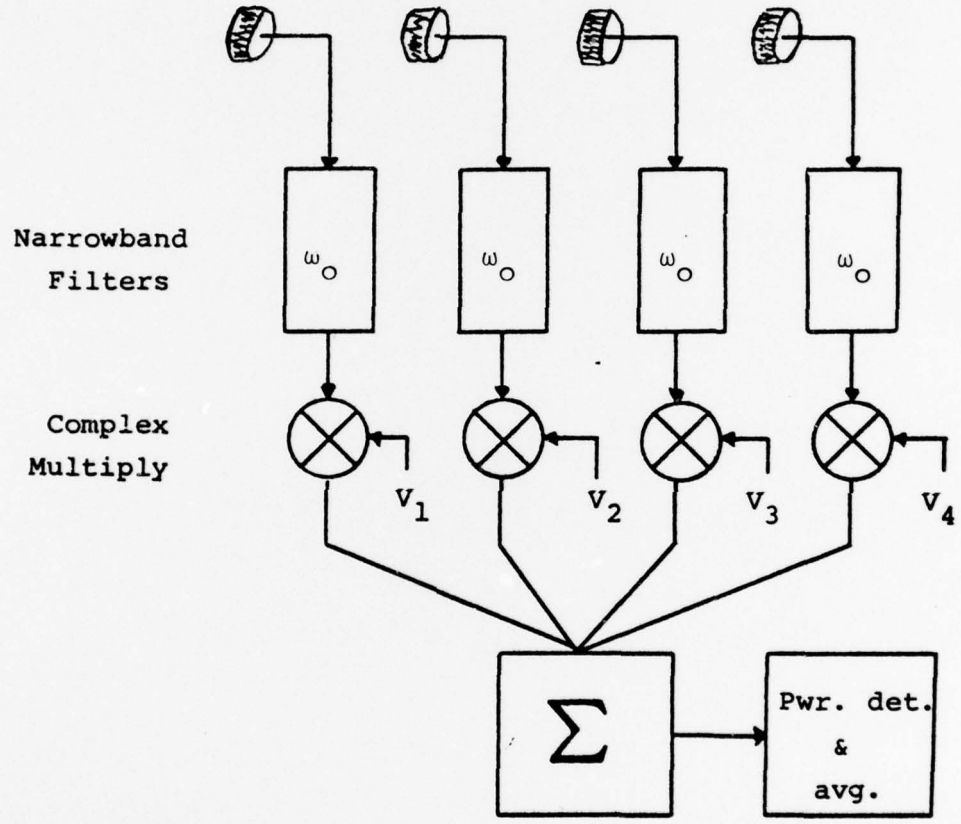

Figure 2.1 Signal Processing to Obtain a Wavenumber-Frequency Spectral Estimate.

The resulting measured wavenumber-frequency spectrum is given by:

$$P_M(k_s,\omega_o) = \frac{dN_e}{2\pi \ell_W} \int_{-\infty}^{\infty} P_o(k,\omega_o)\,|H(k)|^2\,|A(k-k_s)|^2 dk \qquad (2.2)$$

where

$P_o(k,\omega_o)$ is the wavenumber-frequency spectrum of the circumferentially averaged pressure,

$H(k)$ is the element factor representing the response of a single element to wavenumber, k,

and

$A(k)$ is the "array factor" given by,

$$A(k) = \sum_{\ell=1}^{N_e} a_\ell e^{ik(\ell-1)d} \qquad (2.3)$$

In Equation (2.2), the quantity ℓ_W is the white noise loss factor given by,

$$\ell_W = N_e \sum_{\ell=1}^{N_e} |a_\ell|^2 \qquad (2.4)$$

The factor $\frac{2\pi \ell_W}{dN_e}$ represents the equivalent k-space bandwidth of the array factor. That is:

$$\int_{-\pi/d}^{\pi/d} |A(k)|^2 dk = \frac{2\pi \ell_W}{dN_e} \qquad (2.5)$$

Note that the normalization assumed in (2.1) implies $A(0) = 1$.

An estimate of the axisymmetric wavenumber-frequency spectrum, $P_o(k,\omega)$ can be obtained in those regions of k-space which are not significantly distorted by the element and array factors. Qualitatively, the effect of each factor in Equation (2.2) can be sketched as shown in Figure 2.2. There it is shown that the element factor is generally a relatively broad response in k-space, but except for thin elements, significantly attenuates the convective component.

The array factor, on the other hand, has a very narrow response in k-space, centered on the desired wavenumber k_s. The approximate width of the main response lobe is equal to 2π times the reciprocial of the array length. By making the array long enough, it is possible to obtain high resolution spectral estimates. If the wavenumber spectrum were perfectly flat, resolution would not be a significant consideration, however, according to the model proposed by Chase [3], the spectrum changes rapidly with k at low wavenumbers. If the spectral level changes significantly across the main response lobe, the resulting spectral estimate will be biased away from the true value.

Another feature of the array factor which must be considered, is that it is periodic with period equal to 2π times the reciprocal of the element spacing. Thus, in addition to accepting energy from the desired wavenumber, an array of point elements accepts energy equally at the wavenumbers, $k_s \pm 2\pi n/d$, $n = 1,2,\ldots$ For a general array, if there is significant energy in the spectrum at the ambiguous wavenumbers, and if this energy has not been attenuated by the element factor, the resulting measurement will be biased by the ambiguities in the array factor. In the literature on phased arrays, the array factor periodicities

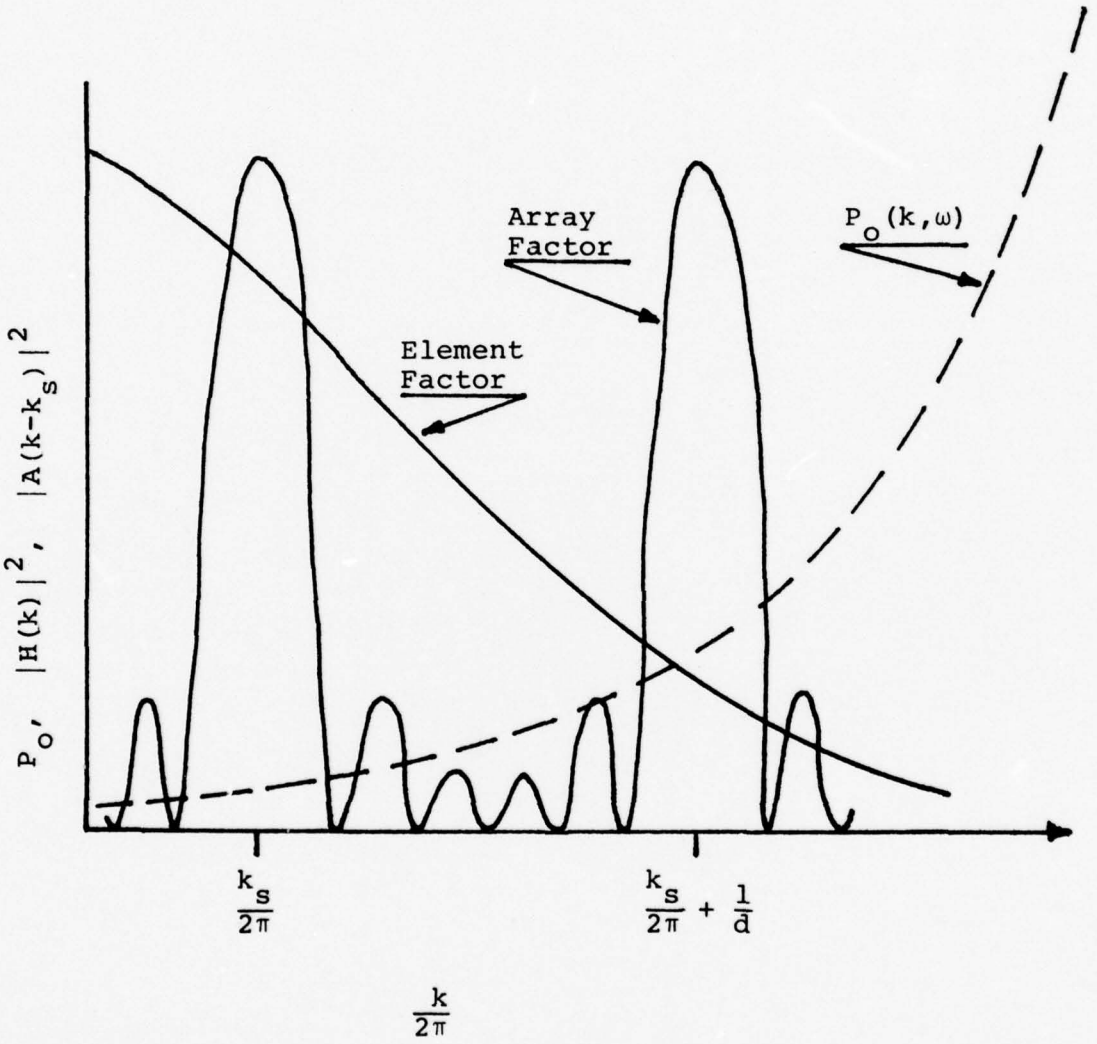

Figure 2.2. Sketch Showing Characteristics of the Array and Element Factors.

are called "grating lobes". In the signal processing literature, the errors produced by the periodicities are called "aliasing errors". Both these terms will be used as appropriate.

Finally, note on Figure 2.2, that between the periodic ambiguities of the array factor, there are sidelobe responses which are usually many dB below the main response. However, if these sidelobes lie within the convective region, they still may pick up significant energy and consequently bias the low wavenumber measurement.

The primary problem of array design is to choose the array parameters to reduce the bias errors described above to an acceptable level. The approach taken in this report is to note that from Equation (2.2), the element factor produces a modified spectrum, $P_o \cdot |H|^2$, which is measured by steering the array factor to various wavenumbers. The element pattern produces two effects. On the negative side, it limits the maximum wavenumber for which unbiased estimates of P_o can be obtained. However, on the positive side, it reduces the dynamic range of the spectrum which is to be measured and thus reduces the requirements on the array sidelobe levels.

Given a particular element size, the product $P_o \cdot |H|^2$ is determined, and then the problem is to choose a high enough spatial sample rate (small enough element spacing) to prevent aliasing errors from distorting the spectrum. Once the element spacing is determined, one must choose a long enough array so that the resolution will be adequate to prevent biases over the rapidly varying portions of the spectrum. Finally, the array weighting

function must be determined so that the array sidelobes will be low enough to prevent biases due to sidelobe leakage.

In general, an exhaustive search for the optimum array characteristics would repeat the above procedure for all possible element widths until the best array was found. In this report the search will be conducted in three stages. First "wafer"* elements are assumed. For such elements it is found that the maximum frequency for which useful measurements can be made depends strongly on the minimum element separation which can be implemented. For a one-eighth inch separation, the maximum frequency is 160 Hz. For one-quarter inch separation, the maximum is 100 Hz.** In the second stage, a center frequency of 100 Hz is assumed and the effect of wider elements with correspondingly greater separation is investigated. At the end of this stage, two nominal array designs will be chosen. In the third stage, the performance of the two nominal designs will be investigated for center frequencies of 50 and 100 Hz. Also in this stage, the effect of relaxed channel-to-channel tolerances is considered. Finally, performance at other tow speeds and frequencies will be discussed.

2.1 Design for Wafer Elements

Figure 2.3 plots the Chase model of P_o for a three inch diameter cylinder towed at 15 kts. The results are

---

*Wafer are so thin that it may be assumed $|H(k)| \simeq 1$ over the region of interest.

**These limits, of course, depend on tow speed and array diameter. U = 15 kts and $2a$ = 3 in was assumed.

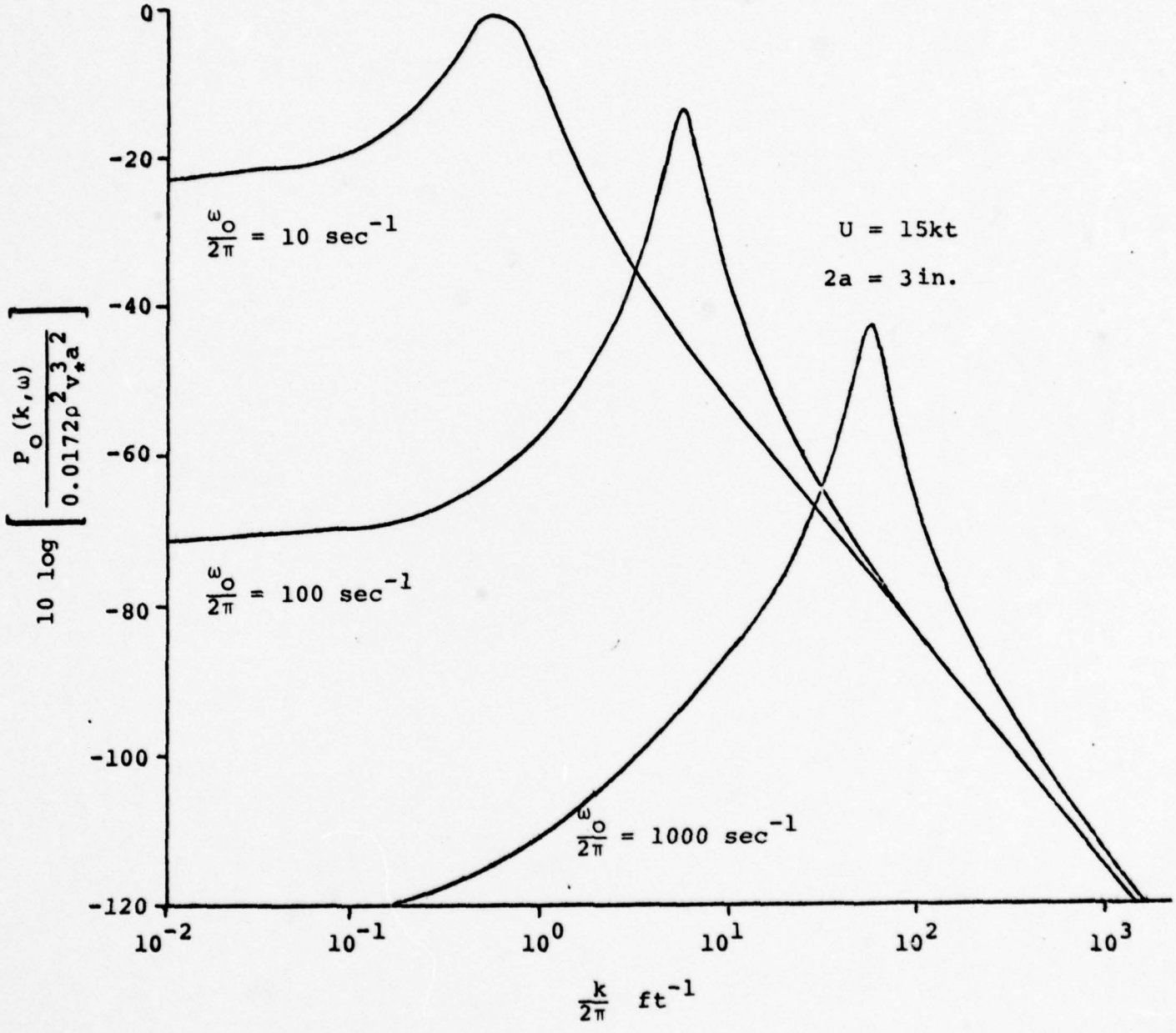

Figure 2.3. Wavenumber-Frequency Spectrum of the Axisymmetric Component of Pressure for a 3 inch Diameter Cylinder.

shown as a function of k with frequency of the narrowband filter, ω_o, as a parameter.

Note that as the center frequency increases, the wavenumber corresponding to the convective peak increases proportionally. At the same time the low wavenumber spectral content decreases more rapidly than does the convective peak, thus producing an increased spectral dynamic range. Both of these characteristics imply that the array design becomes more difficult as ω_o increases. First, as the convective peak moves to higher wavenumber, the elements must be placed closer together to reduce biases produced by aliasing. Second, the greater dynamic range requires better sidelobe control of the array response function which, in turn, implies tighter amplitude, phase, and position tolerances between channels.

Figures 2.4 and 2.5 illustrate the effect of aliasing for two cases. These figures compare the Chase model with a numerical evaluation of Equation (2.2). Note that since the array response is periodic, Equation (2.2) may be written:

$$P_M(k_s,\omega_o) = \frac{dN_e}{2\pi \ell_W} \int_{-\pi/d}^{\pi/d} P_A(k,\omega_o) \, |A(k-k_s)|^2 dk \qquad (2.4)$$

where P_A is the aliased spectrum given by:

$$P_A(k,\omega_o) = \sum_{n=-\infty}^{\infty} P_o(k + \frac{2\pi n}{d},\omega_o) \, |H(k + \frac{2\pi n}{d})|^2 \qquad (2.5)$$

Since only the effects of aliasing are of interest, for this calculation, a long array is assumed so that one has:

$$\frac{dN_e}{2\pi \ell_W} |A(k-k_s)|^2 \simeq \delta(k-k_s) \qquad (2.6)$$

where δ is the Dirac delta function. Thus for Figures 2.4 and 2.5, $P_M(k_s,\omega_o) = P_A(k_s,\omega_o)$. Further the assumption of wafer elements allows the approximation -- $|H(k)|^2 \simeq 1$.*

Figure 2.4 shows that for one inch spacing, the aliased spectrum is representative of P_o only in the region near the convective peak. In this case the aliased spectrum P_A is periodic in k with a period $2\pi \cdot (12) ft^{-1}$. If the element spacing is reduced to one-quarter inch the period increases to $2\pi \cdot (48) ft^{-1}$ and the aliased spectrum is a good representation of the Chase model. Physically, what is happening is that in Figure 2.4, when the array is steered to low wavenumbers, the first grating lobe (ambiguous response) of the array is folding in high spectral levels from near the convective peak and thus masking the low wavenumber energy. In Figure 2.5, when the array is steered to low wavenumber, the first ambiguous response is well beyond the convective ridge where the spectral level is again low, and the folded energy causes a relatively small bias.

In evaluating the aliased spectrum (Eq.(2.5)), it is found that the summation depends almost entirely on the ambiguous response near the convective peak. Thus, Figure 2.3 can be used to estimate the required element spacing for a three inch diameter cylinder. In particular,

---

* In the following figures w denotes the element width and k_B denotes the effective 3 dB array "bandwidth" in k-space. Thus, D=0 is shorthand for the assumption $|H(k)|^2 = 1$, and $k_B = 0$ is shorthand for the assumption (2.6).

$\frac{\omega_o}{2\pi} = 100 \text{ sec}^{-1}$

d = 1 inch

w = 0 inch

$\frac{k_B}{2\pi} = 0 \text{ ft}^{-1}$

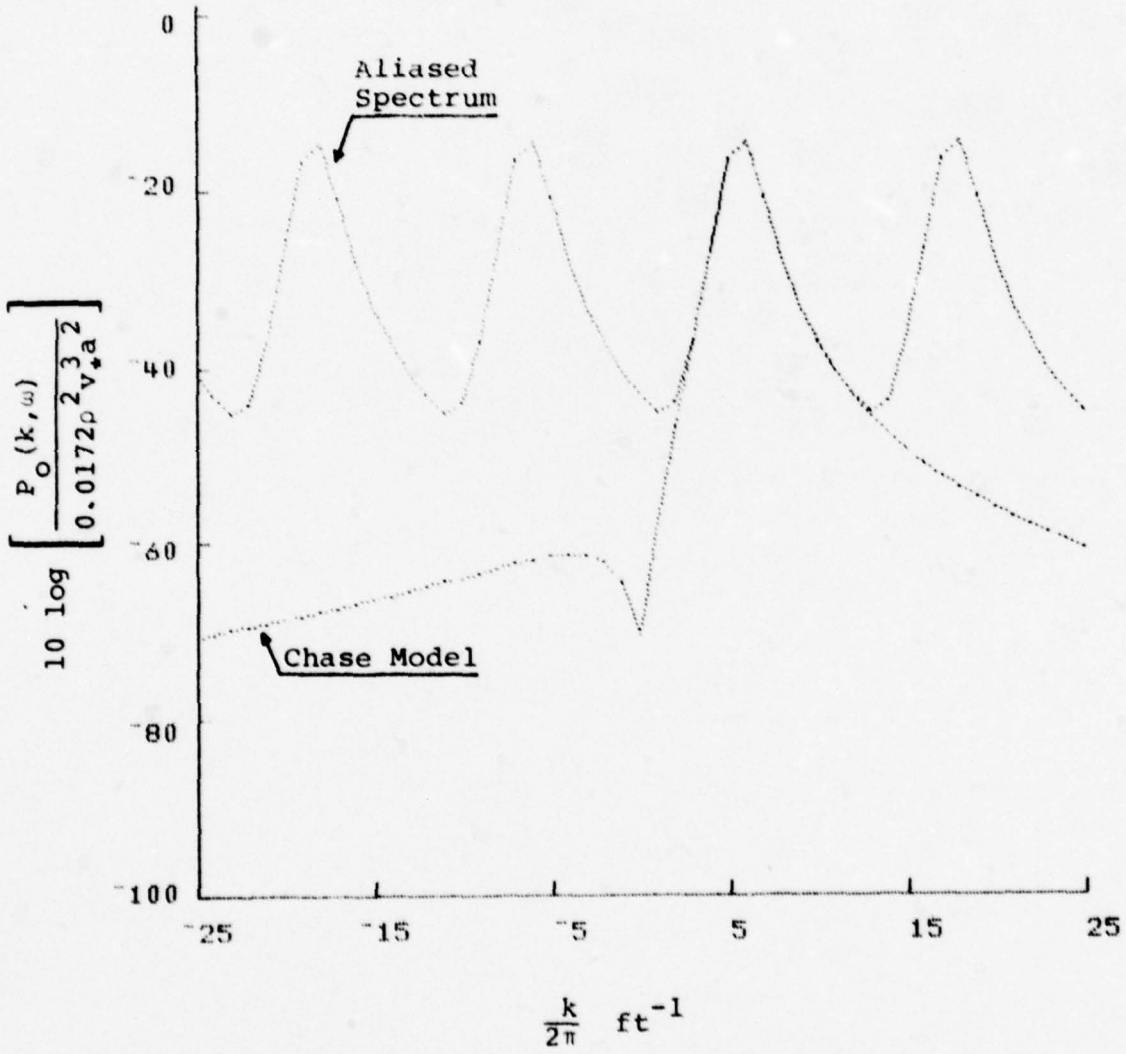

Figure 2.4. Aliasing with 1 inch Spacing and Wafer Elements.

$\frac{\omega_o}{2\pi} = 100 \text{ sec}^{-1}$

d = 1/4 inch

w = 0 inch

$\frac{k_B}{2\pi} = 0 \text{ ft}^{-1}$

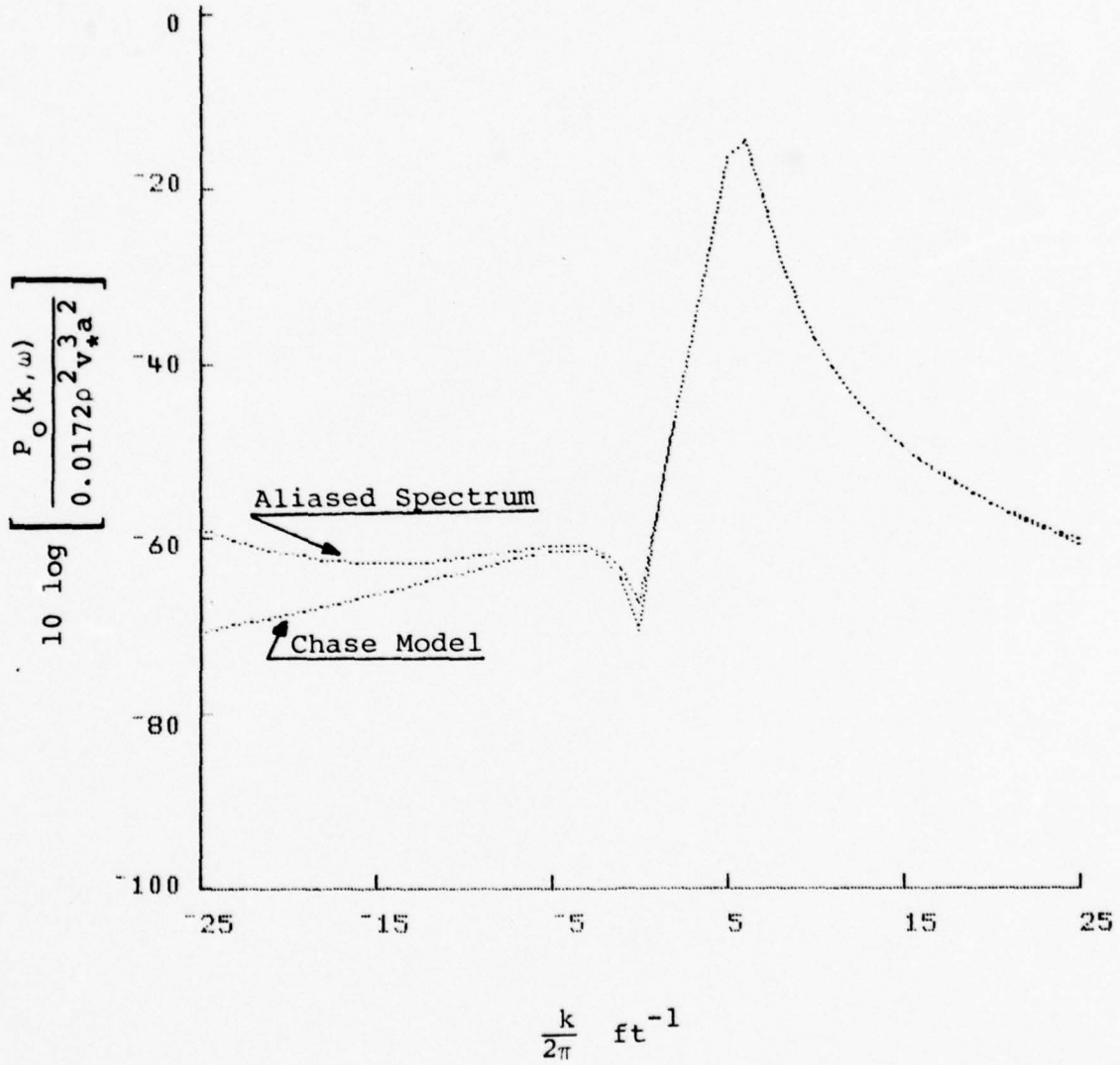

Figure 2.5. Aliasing with 1/4th inch Spacing, and Wafer Elements

at low wavenumber, the major contribution to the measured energy will come from the ambiguous lobe located at $k_s+2\pi/d$. If this lobe lies too close to the convective peak, the low wavenumber measurement will be biased by the ambiguous response. Quantitatively, if a 3 dB bias in the low wavenumber measurement is acceptable, the spectral level at the ambiguous response must be less than or equal to the spectral level at low wavenumbers. Since the spectrum is increasing with wavenumber until the convective peak is reached, this requirement immediately dictates that the first ambiguous response must be well beyond the convective peak. In particular, the element spacing is chosen so that the first ambiguous response is beyond the convective peak and such that the spectral level there is equal to the spectral level at low wavenumber. For example, at a frequency of 100 Hz, the spectral level at low wavenumber is -57 dB relative to the peak. This spectral level is again reached for $(k/2\pi) = 47\ ft^{-1}$ thus the required element spacing is 0.25 in.

The 3 dB criterion represents relatively poor accuracy for the spectral estimate; however since the discussion in the introduction indicates that the current uncertainty in the low wavenumber content may be as high as 20 dB, it is felt that the 3 dB criterion is acceptable. If this is not true, the required spatial sampling rates will be significantly increased.

The computation of the required sampling rate based on the aliasing at low wavenumber is not a general criterion applicable to all spectral shapes. In general, the aliasing error should be estimated at all wavenumbers over the region of interest and the spatial sampling rate should be chosen to control the worst aliasing error.

Computations with the Chase model, however, indicate that the worst aliasing does occur at low wavenumber. The above comment would not be true if we were concerned with the measurement of wavenumbers beyond the convective peak. In particular, the spectral level cannot be measured at wavenumbers greater than one-half the spatial sampling rate (Nyquist rate) away from the convective peak since the aliasing error becomes very large. (See Figure 2.4).

Using these considerations, the required sample rate is plotted versus frequency for a three inch cylinder in Figure 2.6. This figure demonstrates that there is a strong limit to the maximum frequency at which useful measurements can be obtained. For example, if it is assumed that an element spacing of one-eighth inch represents the minimum which could be achieved, then the maximum frequency is limited to about 160 Hz. For one-quarter inch spacing the maximum frequency is about 100 Hz.

The next step in determining the array parameters is to compute the required resolution in k-space which will be related, later, to the required array length. To make this computation, the main response lobe of the array factor is approximated by the Gaussian function over a limited region of k-space near the desired wavenumber k_s. That is,

$$\frac{dN_e}{2\pi \ell_W} |A(k-k_s)|^2 \simeq \frac{1}{\sqrt{2\pi}\sigma_k} \exp\left[-\frac{1}{2}\left(\frac{k-k_s}{\sigma_k}\right)^2 \right], \quad |k-k_s| \leq 3\sigma_k \tag{2.7}$$

where $\sigma_k = (8 \ln 2)^{-1/2} k_B$

and k_B is the 3dB "bandwidth" in k-space.

Figure 2.6. Required Spatial Sample Rate

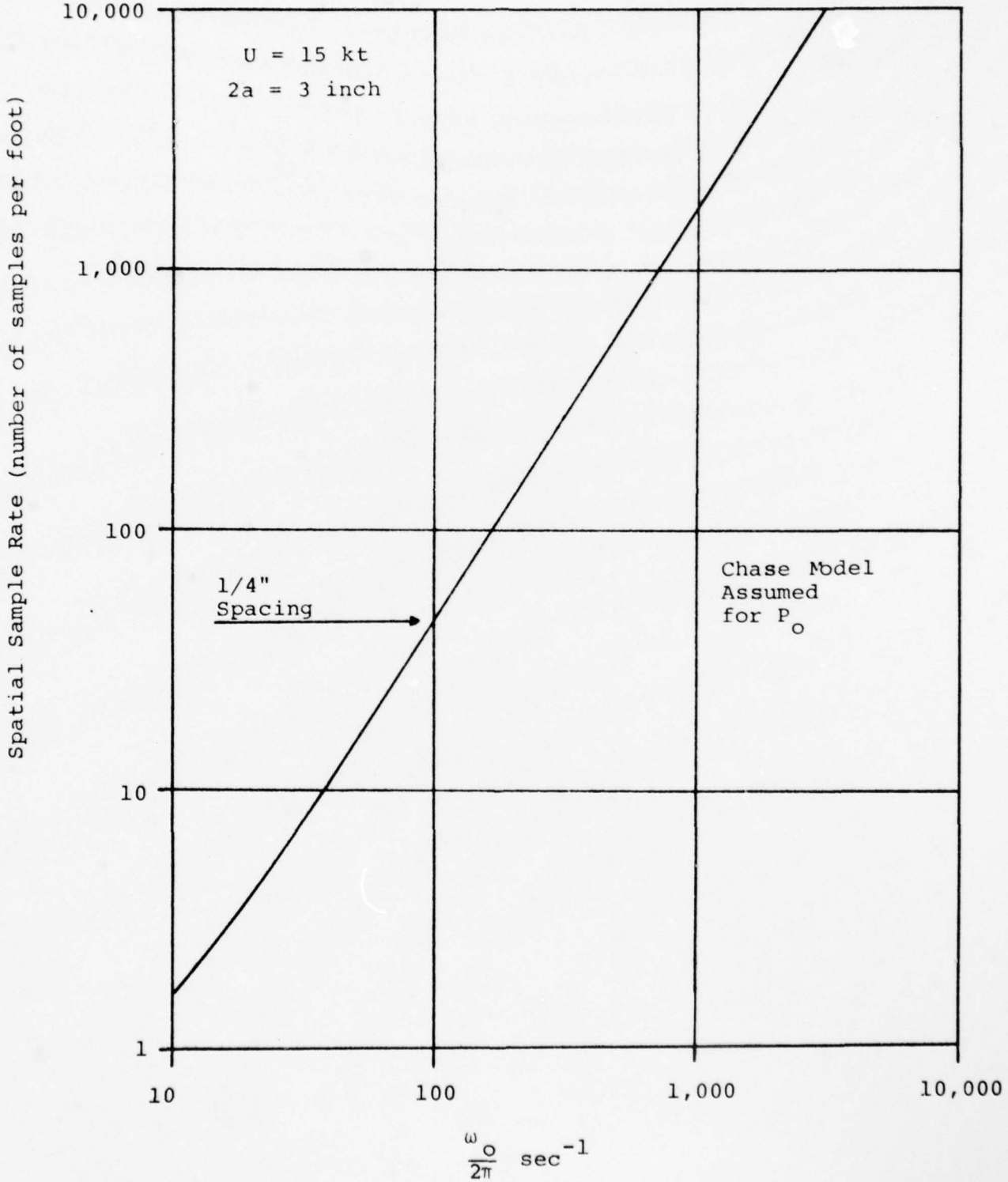

Using this approximation, the measured spectral level can be computed using Equation (2.2) and a numerical quadrature formula to evaluate the integral. Since the quantity being investigated here is the bias produced by the finite resolution of the array factor, the integration is restricted to the main response lobe near the desired wavenumber k_s. The effect of sidelobe response will be considered separately below. The Gaussian approximation to the main response lobe is quite good independent of which array weighting coefficients are used. The major effect of the weighting coefficients is to control the sidelobe level at the expense of increased k-space bandwidth. Thus different array coefficients require different array lengths for the same k_B. As long as the results are given in terms of resolution, they are quite general.

The result of a numerical evaluation of Equation (2.2) using approximation (2.7) for A(k) is shown in Figure 2.7.* For that computation the elements were assumed to be 0.25 in. apart, and the array bandwidth was taken as $(k_B/2\pi) = 1.0$ ft^{-1}. Again, the most significant bias occurs near zero wavenumber. If the bias is plotted versus array bandwidth, for $k_s = 0$, Figure 2.8 results. From that figure, it can be seen that a resolution of $(k_B/2\pi) = 0.65$ ft^{-1} is required to maintain less than 3 dB bias relative to the Chase model. The required array length will depend on the particular weighting coefficients, and these, in turn, depend on the required sidelobe level.

Figure 2.9 can be used to estimate the required sidelobe level of the array factor. As can be seen from

---

* For this and subsequent computations, the "wafer" elements will be assumed to be one quarter inch wide (w=.25in) as this produces negligible distortion of the spectral measurement over the regions of interest.

$\frac{\omega_o}{2\pi}$ = 100 sec^{-1}
d = 1/4 inch
w = 1/4 inch
$\frac{k_B}{2\pi}$ = 1.0 ft^{-1}

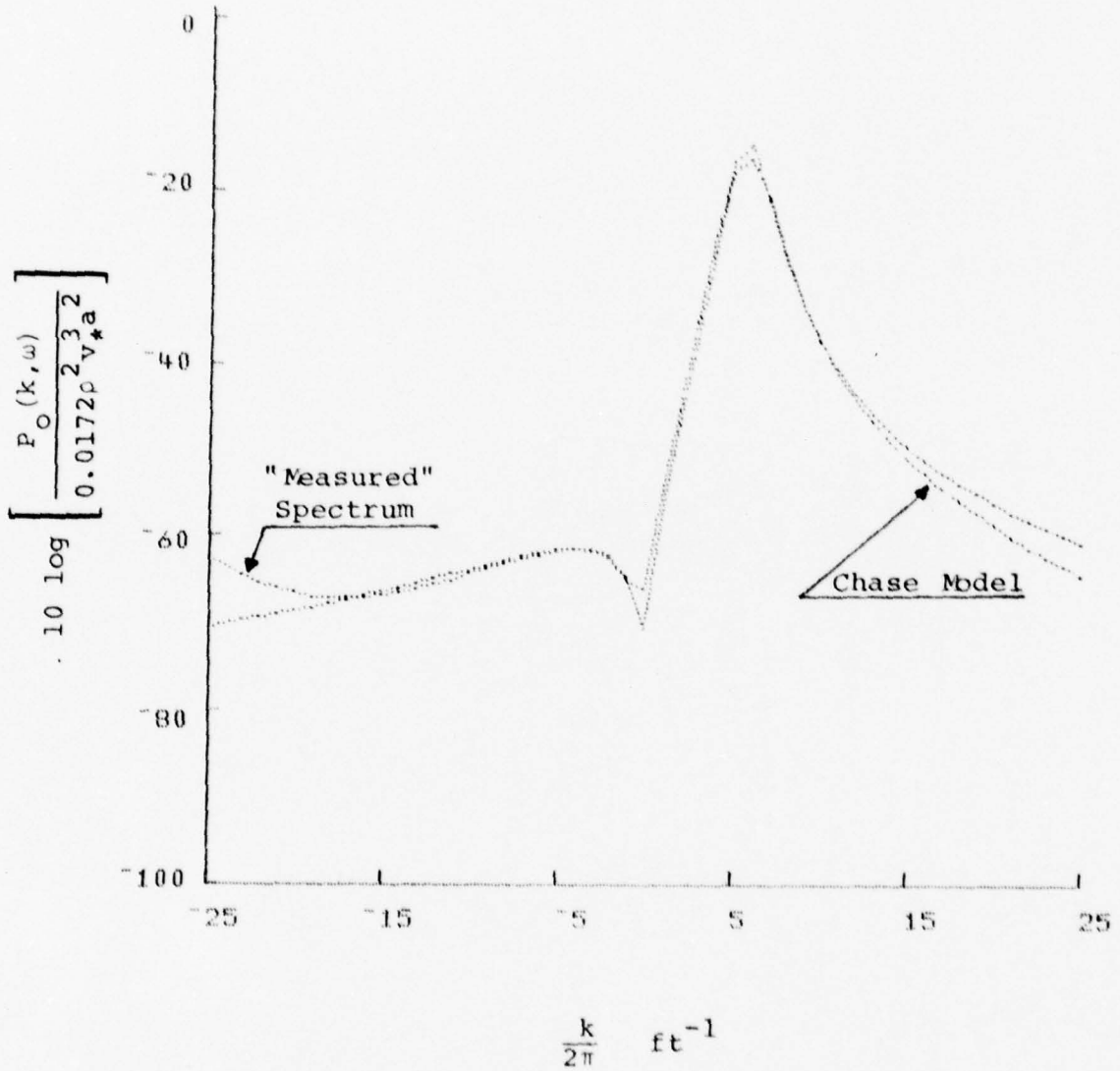

Figure 2.7. Effect of k-space Bandwidth on the Measured Spectrum, P_M.

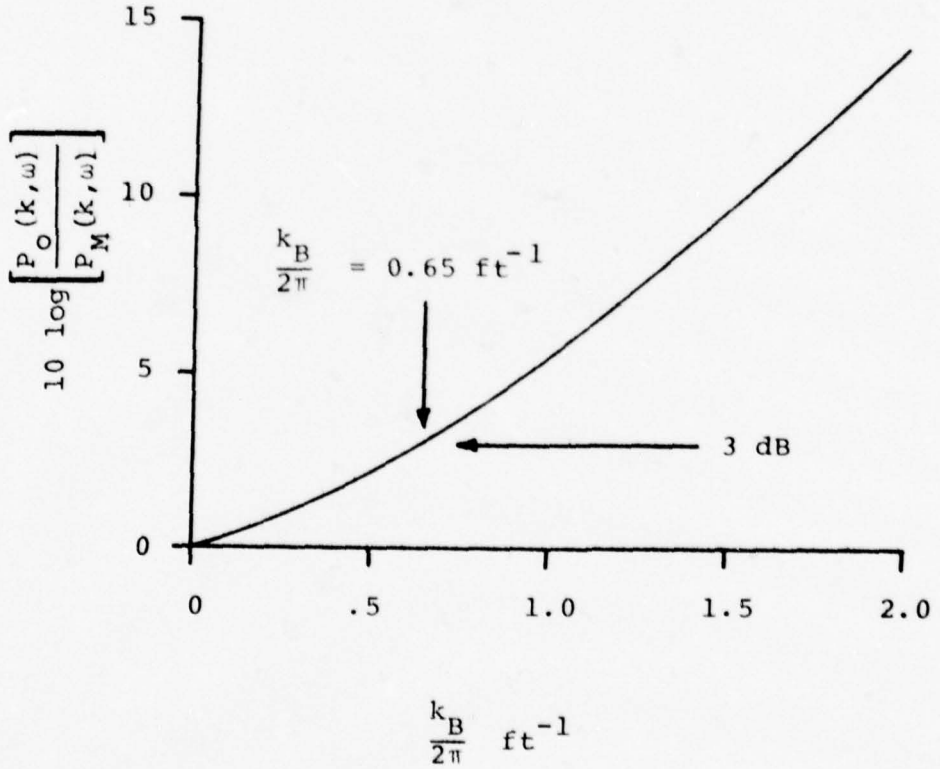

Figure 2.8. Measurement Bias versus k-space Bandwidth (at $k_s = 0$).

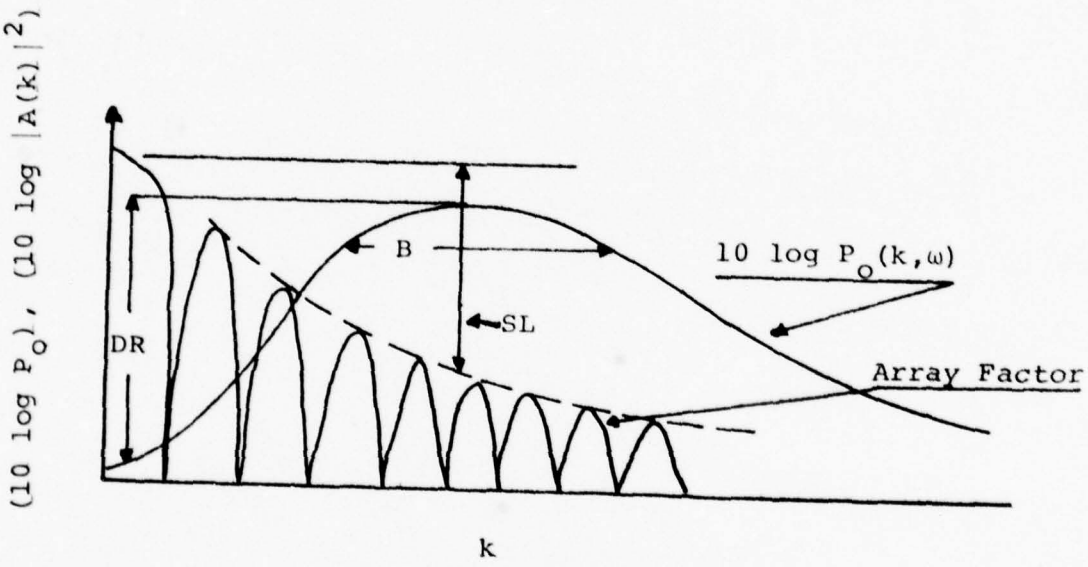

Figure 2.9. Sketch Showing the Parameters needed to Estimate the Required Sidelobe Level.

that figure, this level is a function of the dynamic range of the spectrum, DR, its k-space bandwidth near the convective peak, B, and the array bandwidth k_B. Specifically, the ratio of the leakage through the array sidelobes, P_{SL}, to the spectral level measured at low wavenumber is given approximately by:*

$$10 \log \left[\frac{P_M}{P_{SL}} \right] = SL - DR + 10 \log(k_B/B) \qquad (2.8)$$

where SL is the rms sidelobe level near the convective peak. If the sidelobe leakage is to be less than the measured value, the sidelobe level must satisfy:

$$SL \geq DR + 10 \log(B/k_B) \qquad (2.9)$$

For a 3 inch cylinder towed at 15 kts and a center frequency of 100 Hz, the dynamic range is 57 dB and the bandwidth of the convective peaks is $(B/2\pi) = 1.2$ ft^{-1}. Substituting these values into (2.9) yields a sidelobe requirement of about 60 dB.

Figure 2.10 illustrates the effect of various sidelobe levels using a numerical evaluation of Equation (2.2). For the numerical evaluation, a constant sidelobe level was assumed. Figure 2.10 is consistent with the approximation (2.9) as it indicates that a sidelobe level of 60 dB or

---

* To be specific, the dynamic range is defined as DR = $10 \log[P_o(\omega/U_c,\omega)/P_o(0,\omega)]$ and B is the bandwidth between the 3 dB points around the convective peak. The rms sidelobe level is defined as $SL = -10 \log[(d/2\pi) \int |A(k)|^2 dk]$, where the region of integration is confined to the sidelobe region of A(k).

$\frac{\omega_o}{2\pi}$ = 100 sec^{-1}
d = 1/4 inch
w = 1/4 inch
$\frac{k_B}{2\pi}$ = 1.0 ft^{-1}

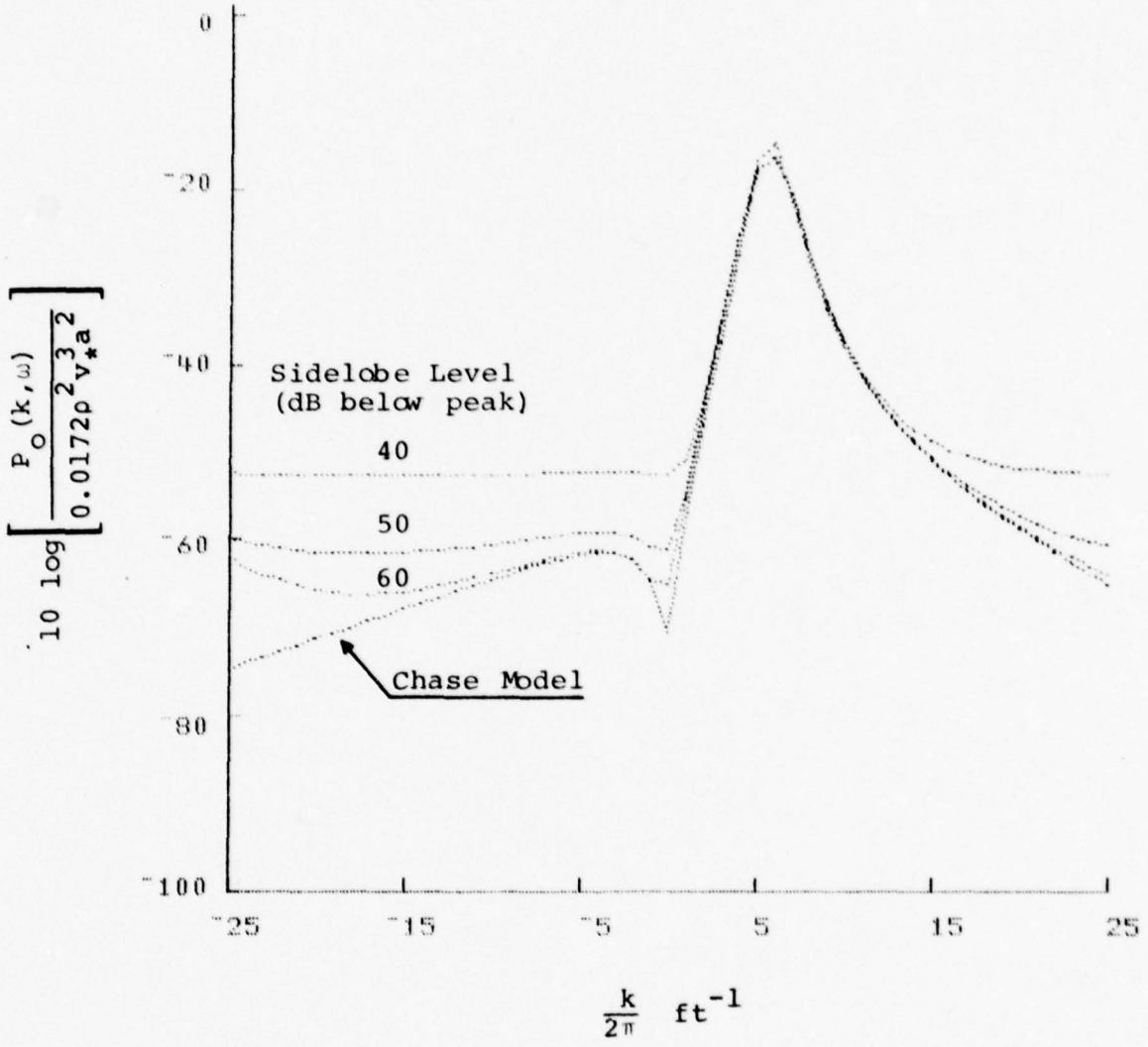

Figure 2.10. Effect of Sidelobes on the Measured Spectrum.

greater is required to prevent sidelobe leakage from the convective peak from masking the low wavenumber content.

This represents a severe sidelobe requirement. Although in theory, Dolph-Chebyshev weighting functions [7], [8], achieve such low levels, tight control on channel-to channel amplitude, phase, and position errors is required. Table 2.1 summarizes the important characteristics of the Dolph-Chebyshev weights. This class of weighting functions should be useful for the current application as they achieve a given peak sidelobe level with minimal broadening in the main response lobe. Table 2.1 lists the "rms" sidelobe level, the 3 dB bandwidth and the white noise loss factor for Dolph-Chebyshev weights as a function of the peak sidelobe level. From that table it appears that the array length required to achieve 60 dB rms sidelobes and a k-space bandwidth of $2\pi \cdot (.65)$ ft^{-1} is 2.2 ft. With an element spacing of 0.25 inches, this corresponds to 105 elements.

As noted earlier the above parameters represent a severe requirement on the amplitude, phase, and position tolerances between the channels. It is shown in Appendix B that the effect of independent amplitude and phase and position errors on the array response is given by:

$$E|B(k,k_s)|^2 = |A_o(k-k_s)|^2(1-\sigma_\phi^2-k^2\sigma_\beta^2) + \frac{\ell_W}{N_e}(\sigma_\varepsilon^2+\sigma_\phi^2+k^2\sigma_\beta^2) \tag{2.10}$$

where

$E|B(k,k_s)|^2$ is the statistical expectation of the array response (squared) which

TABLE 2.1

ARRAY FACTOR CHARACTERISTICS
FOR DOLPH-CHEBYSHEV WEIGHTING
COEFFICIENTS

Peak Sidelobe Level (dB)	rms Sidelobe Level (dB) (approx)	Normalized White Noise Loss Factor	Normalized 3-dB Bandwidth $\left(\frac{N_e dk_B}{2\pi}\right)$
25	28	1.09	1.01
30	33	1.14	1.07
35	38	1.21	1.13
40	43	1.29	1.20
50	53	1.39	1.33
60	63	1.51	1.44
70	73	1.62	1.55
80	83	1.73	1.65

has been perturbed by the amplitude phase and position errors,

$A_o(k-k_s)$ is the unperturbed array factor, (It is assumed that $A_o(k)$ has been normalized so that $A_o(0) = 1$)

ℓ_W is the white noise loss factor for the particular weights used (column 3 in Table 2.1)

N_e is the number of elements,

σ_ϕ is the rms phase error,

σ_ε is the rms amplitude error as a ratio (i.e., $\varepsilon_i=(\delta a_i)/a_i$),

and σ_β is the rms positional error.

The 60 dB sidelobe requirement must be satisfied at the convective peak with the array steered to zero, thus one must have $E|B(\omega/U_c,0)|^2 < 10^{-6}$. If the errors are distributed "equally" between the three sources, one must have:

$$\frac{\omega}{U_c}\sigma_\beta = \sigma_\phi = \sigma_\varepsilon = 0.0049 \qquad (2.11)$$

That is, the phase-error must be less than .28 deg. rms, the amplitude error must be less than 0.042 dB* rms and the position error must be less than 1.6×10^{-3} in.

---

* It is generally useful to give amplitude tolerances in dB as these tolerances are directly relatable to tolerances on the preamp and amplifier gains on each hydrophone channel. To convert to variance of the dB value (say of the amplifier gain) note that for small errors, gain variations are related to fractional amplitude variations as:

$$\Delta G = 20 \log \frac{a_\ell}{a_\ell^\circ} = 8.68 \ln \frac{a_\ell}{a_\ell^\circ}$$

$$= 8.68 \ln(1+\varepsilon_\ell) \simeq 8.68\varepsilon_\ell$$

thus $\sigma_G \simeq 8.68\sigma_\varepsilon$

In summary, the design based on wafer elements requires 105 one-quarter inch elements at the same spacing. The array length is about 2.2 ft. Sidelobe levels of 60 dB are required which imply channel-to-channel tolerances of -- σ_G = .042 dB, σ_ϕ = .29 deg., σ_β = 1.6 mils. These tolerances will be difficult to achieve. It should be remembered however, that they represent residual variations <u>after</u> calibration. A fixed amplitude, phase or spacing error will have a negligible effect on the spectral measurement. If the errors are uniformly distributed between maximum limits the above rms errors correspond to $|\Delta G| \leq .07$ dB, $|\Delta\phi| \leq 0.5$ deg., $|\Delta\beta| \leq 2.8$ mils. The required number of channels is large, and the k-space bandwidth of $(k_B/2\pi) = 0.65$ ft^{-1} is marginal as will be seen later.

2.2 Effect of Element Length

The results of Section 2.1 indicate that an array design with wafer elements will require both tight channel-to-channel tolerances and a large number of elements to achieve a good low-wavenumber measurement capability. In this section, designs based on wider elements will be considered. Wider elements have a narrower response in k-space, which has the effect of reducing the required spectral dynamic range, at the expense of reducing the maximum k to which unbiased measurements can be made.

In [1], two approaches to rejecting the convective peak were considered. The first approach was based on placing the peak far out on the sidelobes of the element pattern. This approach was rejected as it leads to very long elements (5-20 ft).

The second approach was based on choosing the element width to place the first null of the element pattern near the convective peak. The objective was to reduce the spectral dynamic range and thus ease the channel-to-channel tolerance requirements. The argument, unfortunately, is fallacious.

As an example, it was found that at U = 15 kt, $2a = 3$ in, and $(\omega/2\pi) = 100$ sec^{-1}, a two inch element was required to place the first null near the convective peak. However, to prevent significant aliasing the modified spectrum had to be over sampled at one to two samples per inch. It was proposed that the over sampling could be accomplished by summing overlapping groups of smaller elements thus giving an effective element size of two inches with samples spaced less than two inches apart. For example, if one-half inch physical elements are used, overlapping groups of four can provide an effective element length of two inches with samples every one-half inch.

The fallacy is that now, the array consists of one-half inch elements not two inch elements. The spectral dynamic range is that of half-inch elements. The correct way of viewing the problem is to note that, the process of summing overlapping groups of elements and then applying weighting factors to the groups is equivalent to applying a <u>modified</u> set of weights to the original element outputs. The only virtue of the modified weights is that they have a very low sidelobe level in the neighborhood of the convective peak. However, their tolerance to amplitude, phase, and position errors is no better than say Dolph-Chebyshev weights. In particular, note that from Equation 2.10, the major dependence of the sidelobe error on the weights is

in the term ℓ_W. This quantity does not change greatly between different sets of weights; thus the bias in the array factor will be about the same for the modified weights as for an equivalent set of Dolph-Chebyshev weights. The tolerance requirements are also the same. In the following discussion, it will be assumed that the element width and spacing are equal.

The first step in estimating the effect of the element width is to compute the difference between the Chase model and the aliased spectrum (as modified by the element factor, Eq. 2.5). Figure 2.11 illustrates the results of this computation. There the region in k-space over which the aliased spectrum is not more than 3 dB greater than the Chase model is plotted versus element width. For small elements, the region of unbiased measurement is $|k/2\pi| \lesssim 1/2W$. Note that as the element width and spacing increases, the region of valid measurements is correspondingly reduced. Since the most of the spectral energy is concentrated near the convective peak, the measurement interval tends to be centered around this peak. For one-inch elements, the convective peak is reduced about 3 dB. For larger elements, the aliasing error increases rapidly and the measurement interval is rapidly limited to the acoustic region. The maximum element size which yields a measurement interval beyond the acoustic region is about 1.4 in.

Figure 2.12 shows the spectral dynamic range versus element size. Note that this range does not decrease significantly until the element size exceeds 1.4 in. That is, if the element length is chosen large enough to significantly reduce the spectral peak, the corresponding aliasing errors have reduced the measurement interval to

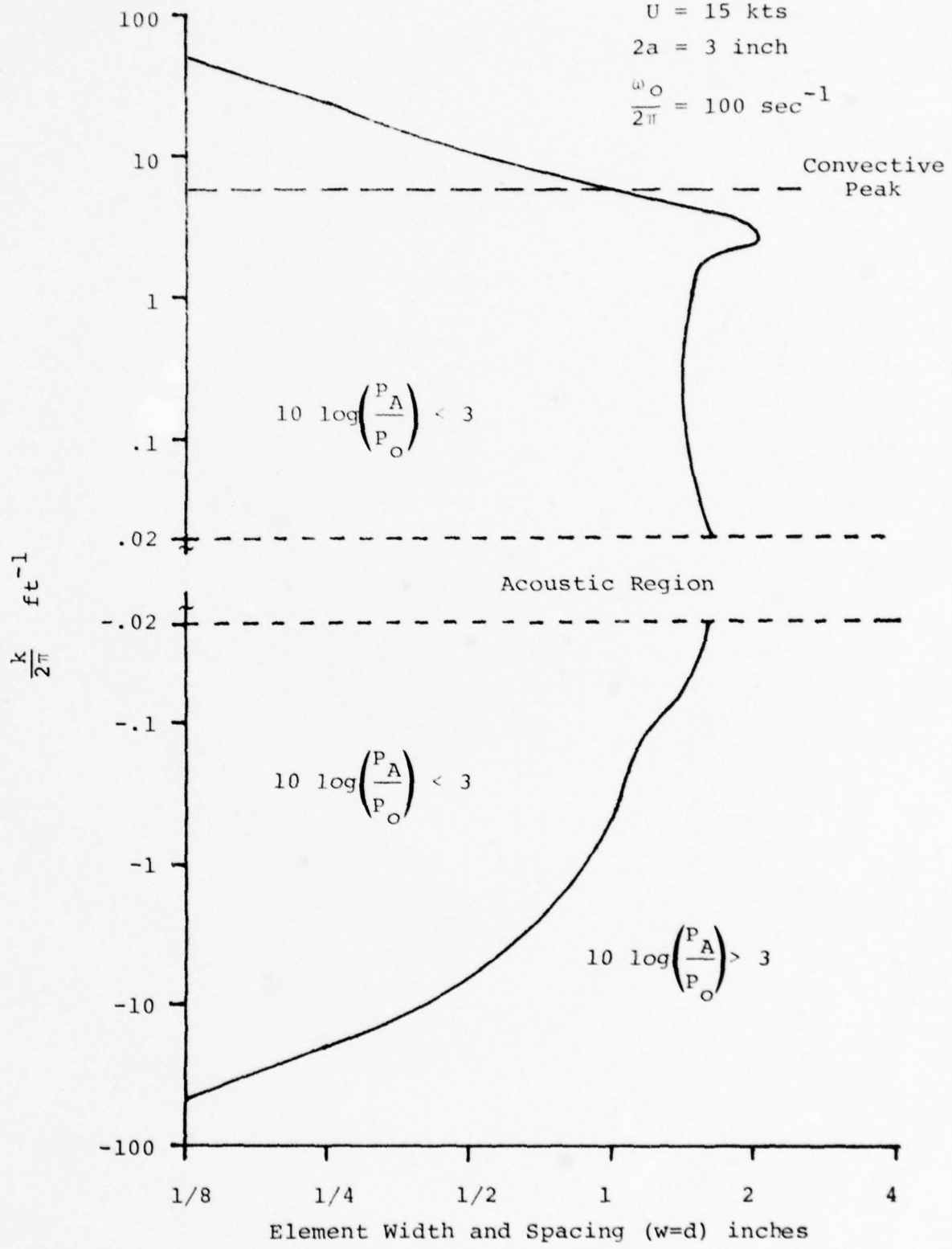

Figure 2.11. Measurement Interval as a Function of Element Width (w=d).

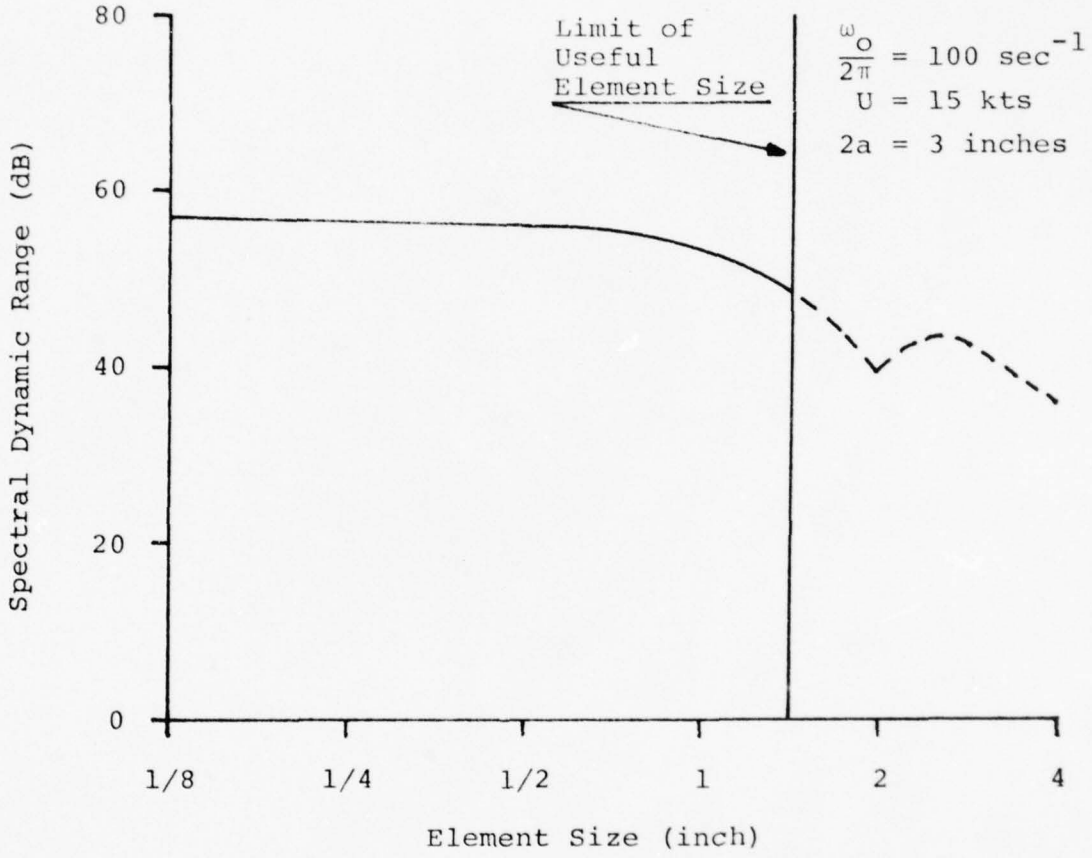

Figure 2.12. Spectral Dynamic Range Versus Element Size.

the acoustic region.

Figure 2.13 shows the number of channels required to achieve $(k_B/2\pi) = 0.65$ ft^{-1} and Figure 2.14 shows the required channel-to-channel tolerances, Dolph-Chebyshev weights are assumed. The least severe tolerances for the least number of elements occurs at w = 1.4 in. This unfortunately is a spurious optimum since its usefulness depends on carefully tailoring the element pattern to the spectrum to be measured. For the remaining calculations a somewhat more conservative maximum element width of 1.2 in. is assumed.

At the other end, the channel tolerances can be eased by using more elements. However, the tolerances increase as $1/\sqrt{N_e}$; thus a large number of channels is required to significantly relax the tolerances. Note that decreasing the element size from one inch to one-half inch has a negligible effect on the required tolerances. This is due to a 2 dB increase in the spectral dynamic range which nearly compensates the increased number of elements.

Figures 2.13 and 2.14 do not indicate the true tradeoffs between element width, number of elements and channel-to-channel tolerances. In particular, those figures were constructed for a constant k-space bandwidth of $(k_B/2\pi) = 0.65$ ft^{-1}. Recall that this is the <u>maximum</u> allowed k-space bandwidth. There is no penalty incurred for decreasing this bandwidth by using a longer array. In fact, from Figure 2.8, decreasing the bandwidth will reduce the bias due to nonzero mainlobe width and improve array performance. Thus if the channel-to-channel tolerances must be relaxed by using more channels, it is more advantageous

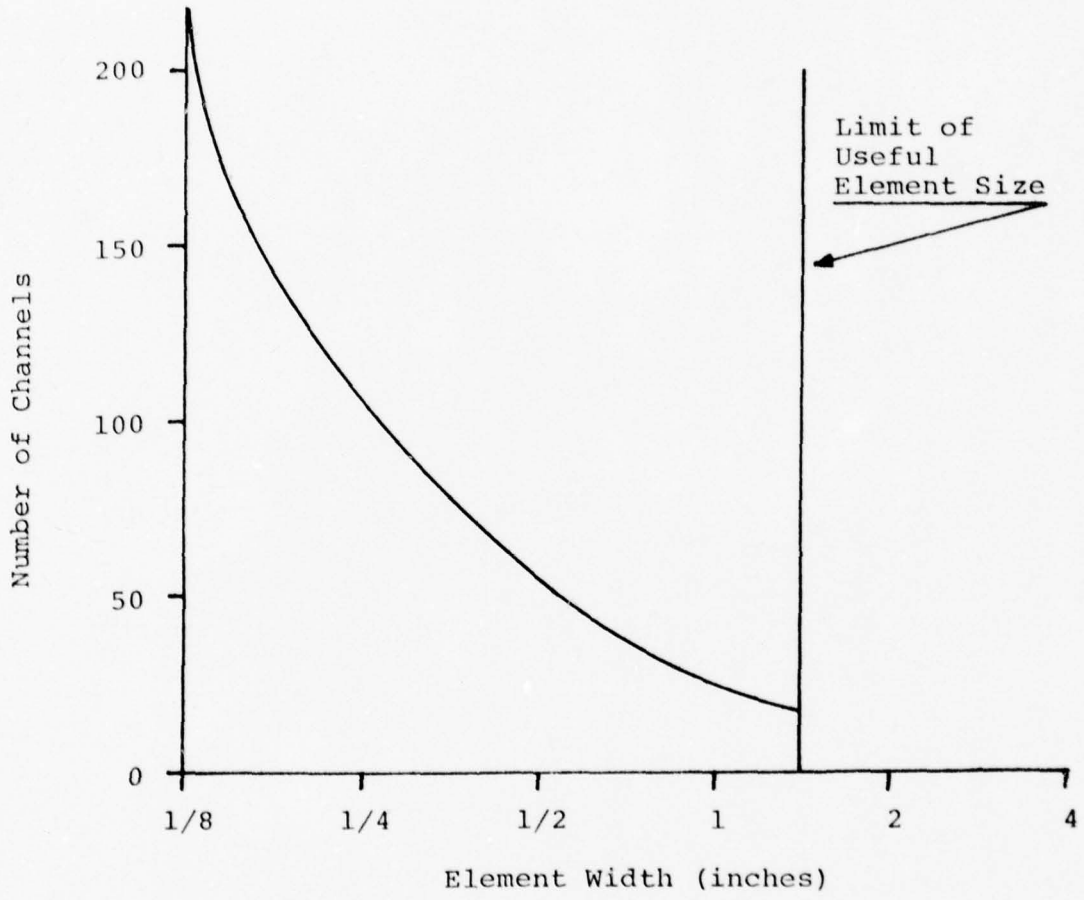

Figure 2.13. Number of Channels Required to Achieve $(k_B/2\pi) = 0.65$ ft^{-1}.

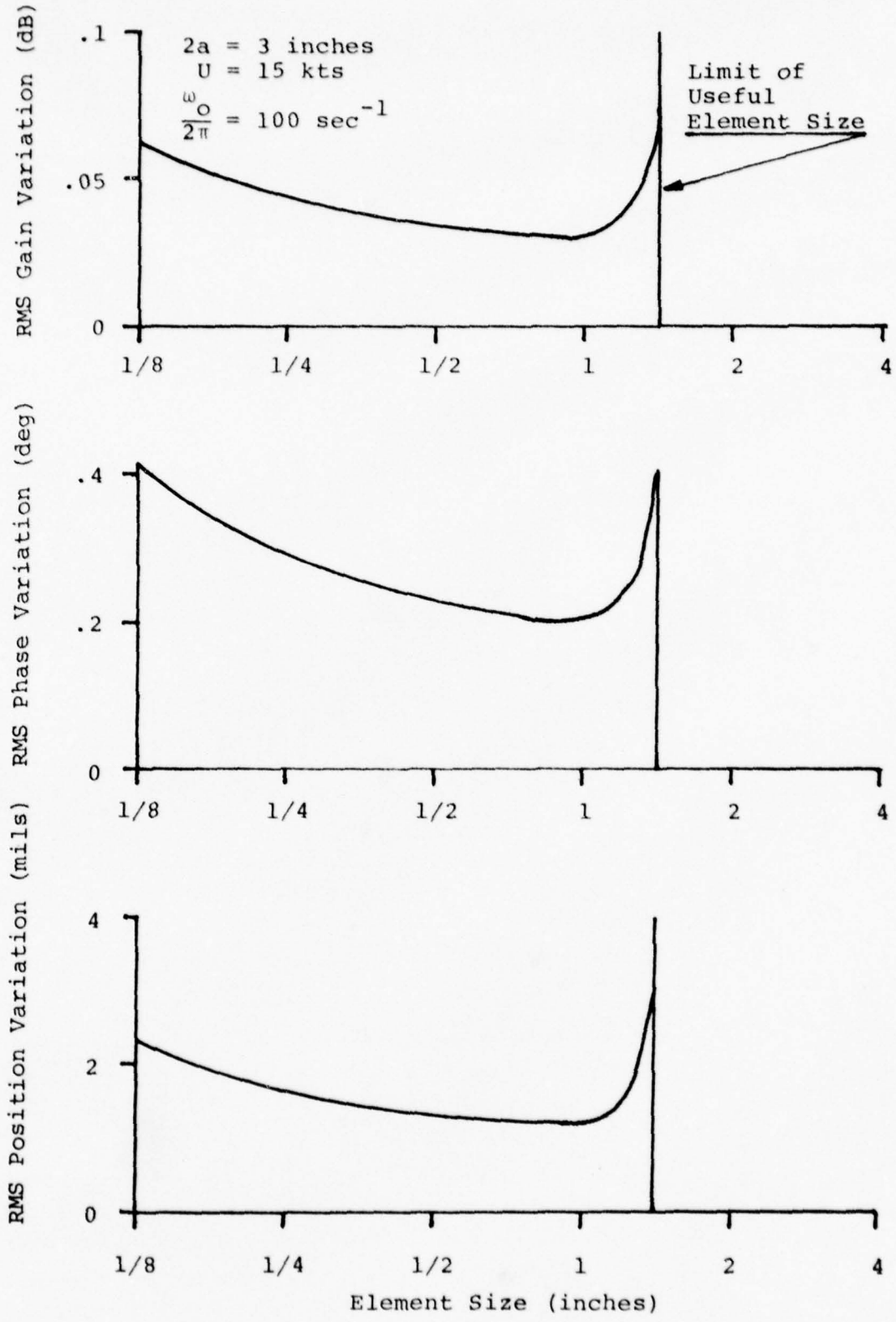

Figure 2.14. Required Channel-to-Channel Tolerances versus Element Size.

to use the largest possible element size and increase the array length accordingly rather than use smaller elements. This is demonstrated in Figure 2.15, where the phase tolerance is plotted versus the number of elements with element width as a parameter.

Figure 2.15 gives the relation between the required number of channels and the required tolerances. If either limit is known the other may be estimated from that figure. Currently neither limit is known. Flush mounted elements of the type indicated in Figure 1.1 have never been built and calibrated in situ, therefore there is no directly applicable previous experience which can be used to estimate achievable tolerance limits. Secondly, at this preliminary design stage, it is not known whether existing tow cable and telemetry systems will be used or new ones will be built. Thus the number of channels available is not known.

The approach taken here will be to "ballpark" the achievable tolerances with optimistic estimates. In particular, it will be assumed that the maximum gain variation can be held to $\pm$ 0.1 dB, the maximum phase variation is $\pm$ 0.5 deg. and the maximum relative position error is $\pm$ 3 mils. If the errors are uniformly distributed between their maximums, the corresponding rms errors are: σ_G = .058 dB, σ_ϕ = .29 deg., and σ_β = 1.7 mils. These tolerances are optimistic, the gain and phase tolerances are two to three times tighter than typical specifications for acoustic modules. The justification for assuming these low values is that they are intended to represent tolerances after calibration corrections have been applied.

From Figure 2.15, the above tolerances imply 35 to 40 elements will be required to make low wavenumber

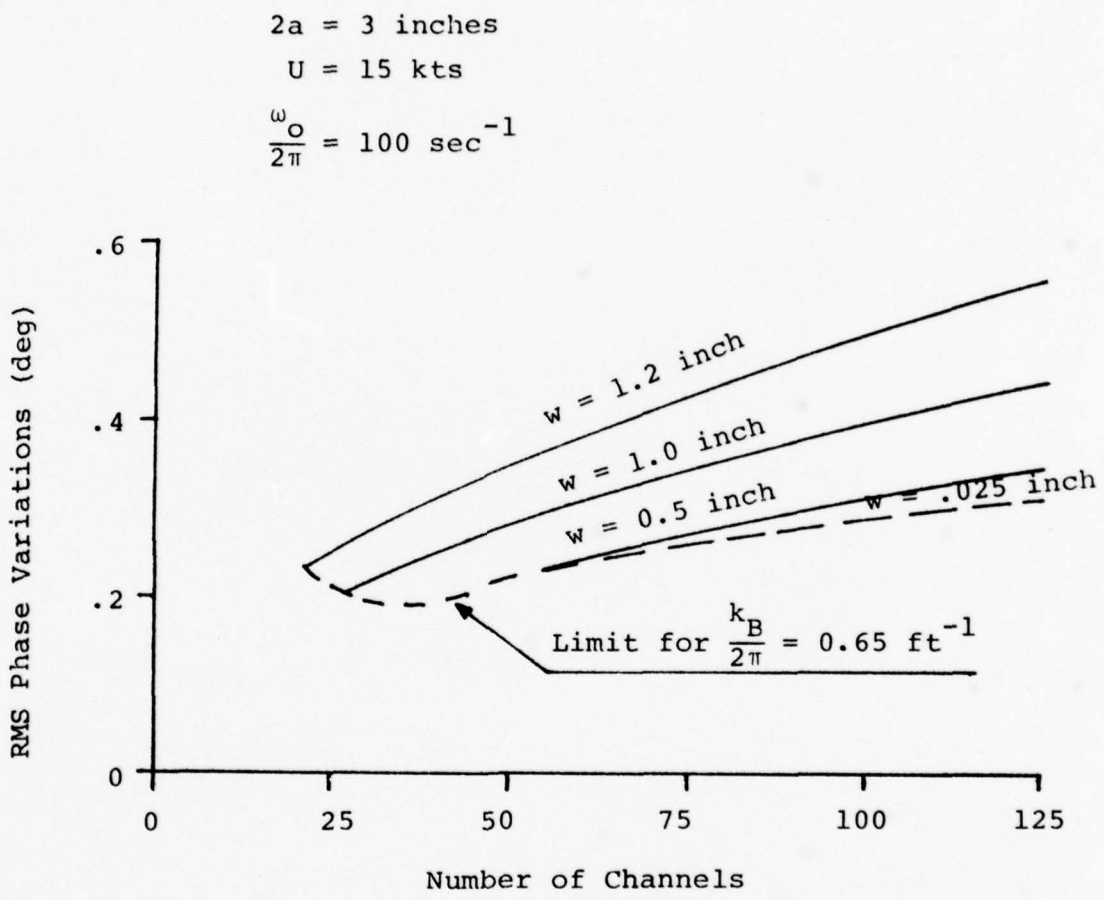

Figure 2.15. Channel-to-Channel Phase Tolerance versus Number of Channels

measurements. This fact also influenced the choice of the assumed tolerance limits as it is unlikely that the number of channels available will greatly exceed 40. For comparison, the performance of a design based on 20 elements with tolerances which are smaller by $\sqrt{2}$ will also be considered.

Figures 2.16 through 2.23 plot the measured spectrum as computed from a numerical evaluation of Equation 2.2 in comparison with the Chase model. Evaluations were made for two arrays at two different frequencies -- 50 Hz and 100 Hz. Additionally, computations were made for sidelobe levels corresponding to the "desired" tolerances and for tolerances which have been increased (relaxed) by $\sqrt{2}$. In those figures, σ is the common tolerance: $\sigma = \sigma_\phi = \sigma_\varepsilon = (\omega/U_c)\sigma_\beta$. Note also that the abscissa is a "lin-log" scale. That is, the scale is proportional to $(\text{sgn } k)\log|k|$ for $|k/2\pi| > .01$ and is linear for $|k/2\pi| \leq 0.01$, where "sgn" is the signum (or sign) function.

First, it should be noted that the "prefered" array at its design frequency of 100 Hz has a bias of about 6 dB in the low-wavenumber measurement. (See Figure 2.16) Since the array was designed to achieve a nominal 3 dB accuracy or better it is reasonable to ask why the bias is so large. The answer is that the array was designed so that each component of the total bias was 3 dB or less. The total error is greater. In particular, it can be shown that at zero wavenumber the bias due to aliasing is 0 dB, the bias due to the finite k-space bandwidth is 1.7 dB (See Figure 2.8) for $(k_B/2\pi) = .36$ ft^{-1} and the bias due the sidelobe leakage is 3.5 dB (Eq. 2.8 and 2.10). The "power sum" of these biases is 5.7 dB as seen in Figure 2.16.

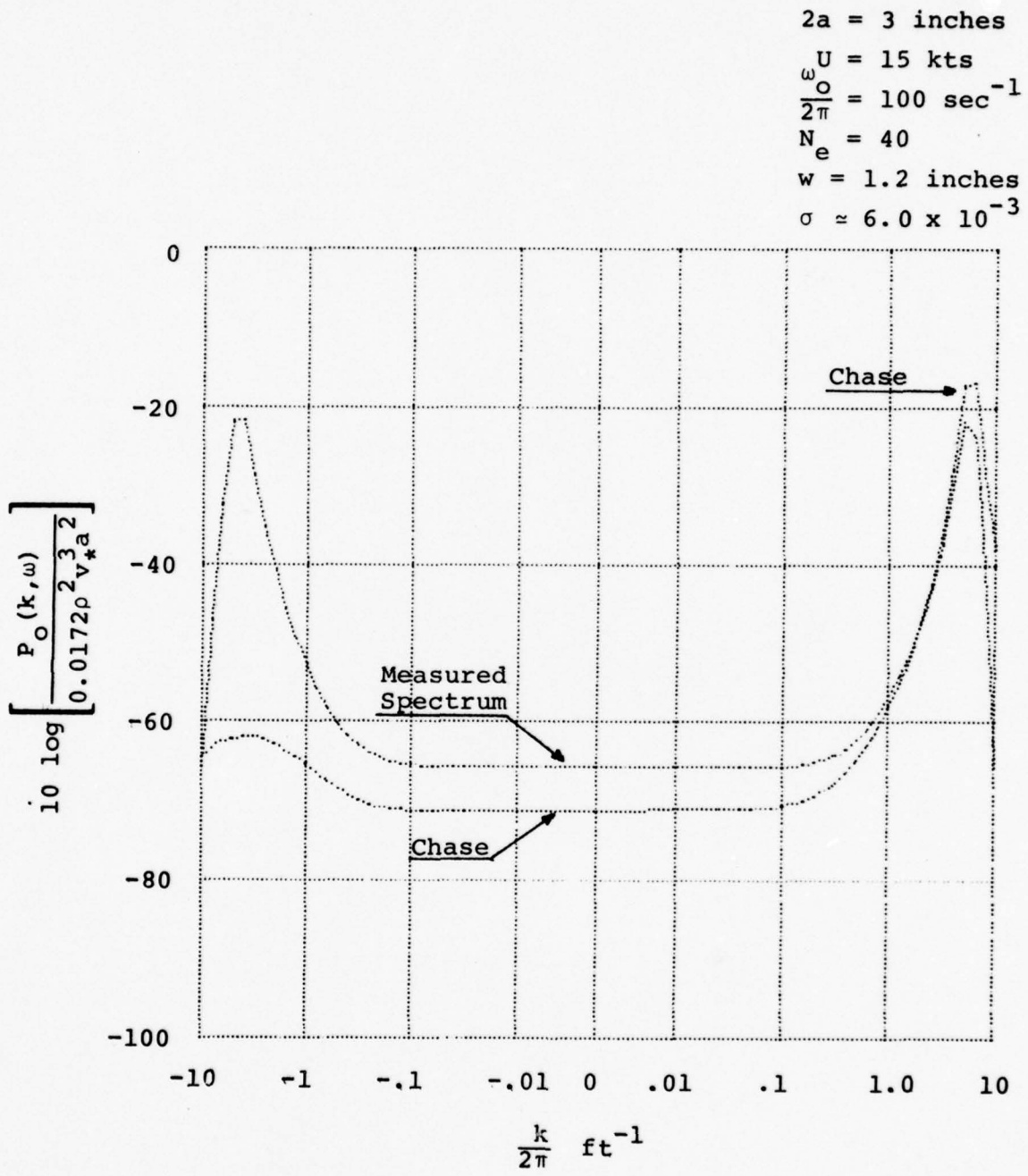

Figure 2.16. Comparison of the Measured Spectrum with the Chase Model (Large Array, Tight Tolerance, 100 Hz).

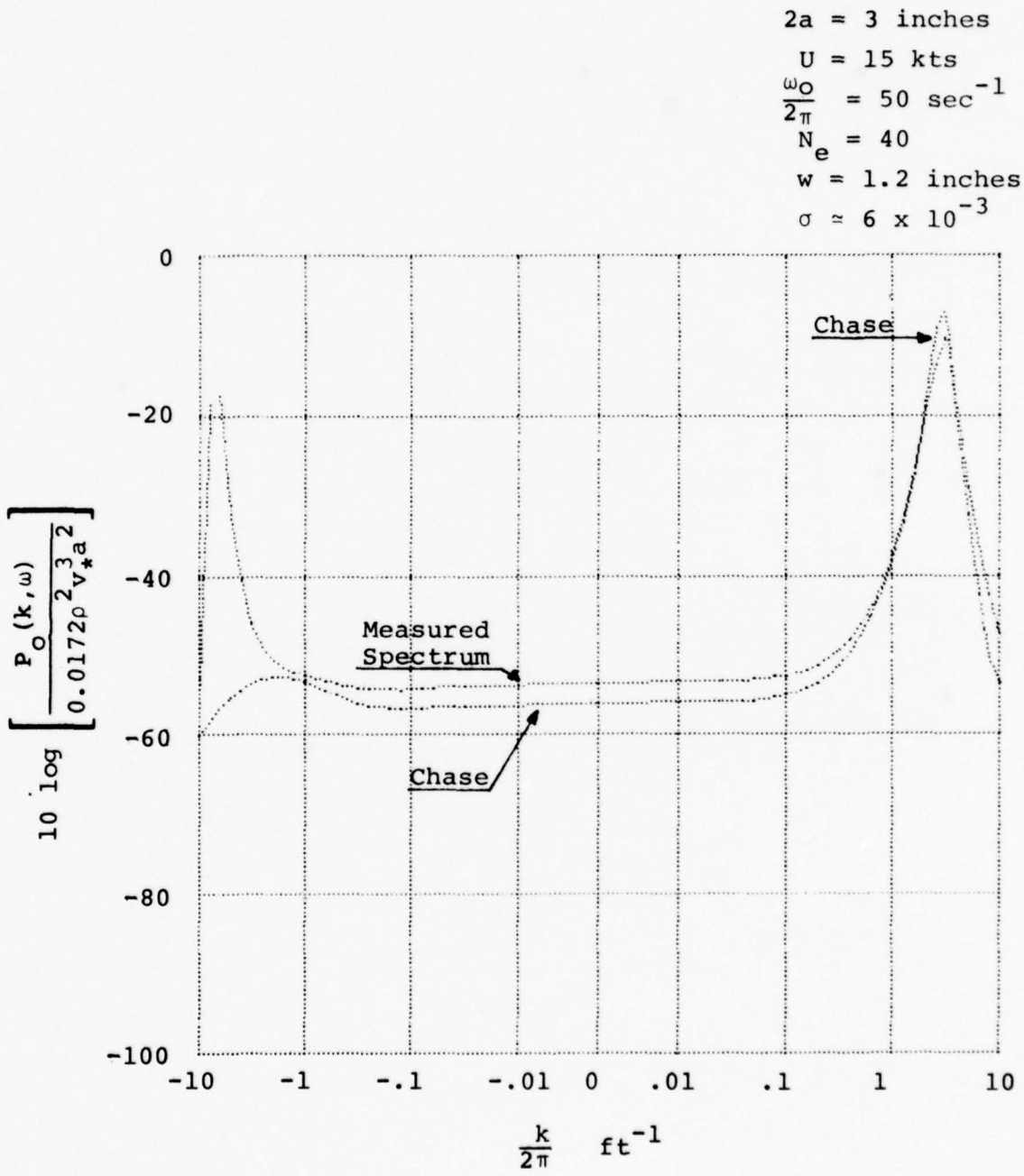

Figure 2.17. Comparison of the Measured Spectrum with the Chase Model (Large Array, Tight Tolerances, 50 Hz).

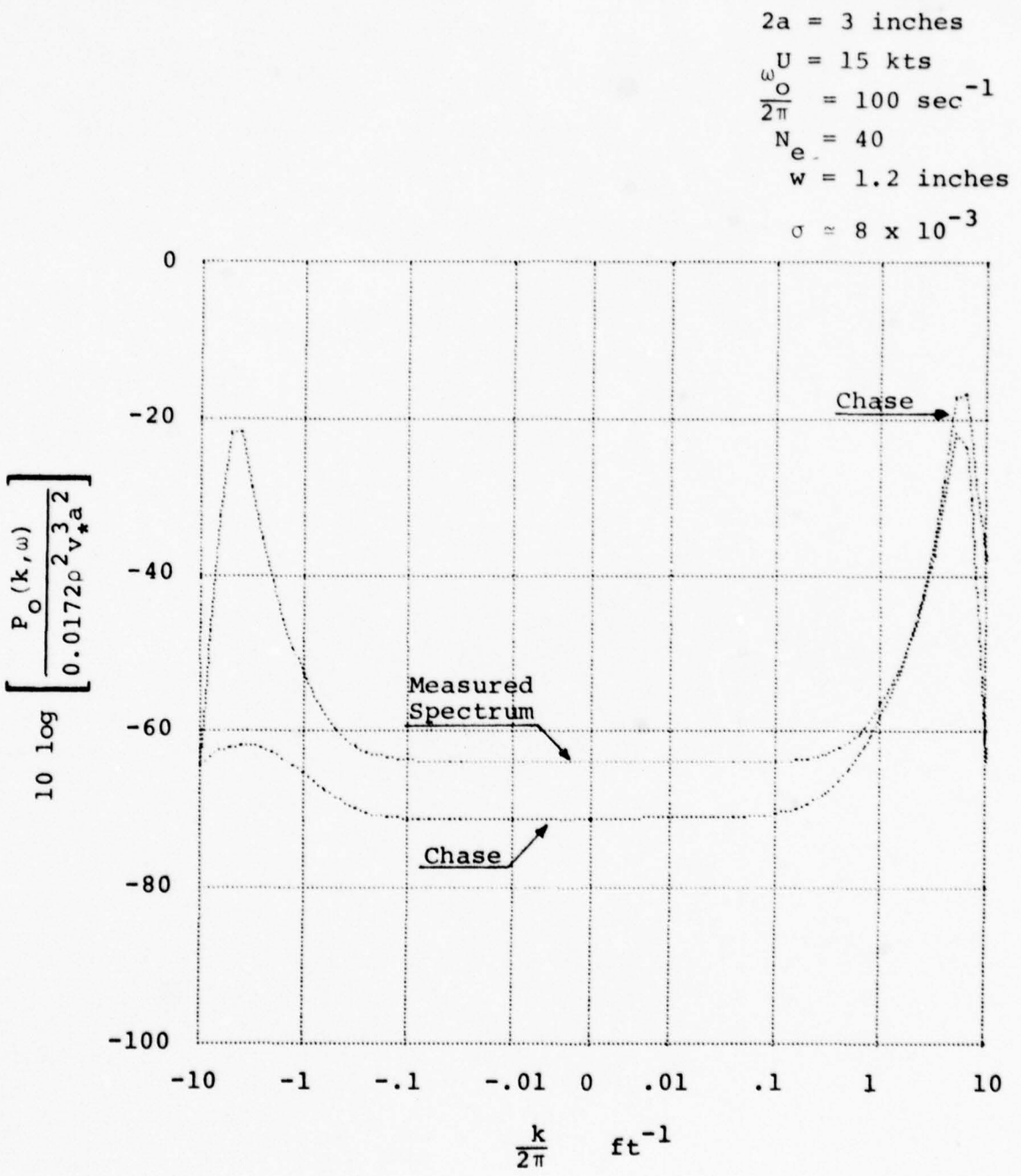

Figure 2.18. Comparison of the Measured Spectrum with the Chase Model (Large Array, Relaxed Tolerances, 100 Hz).

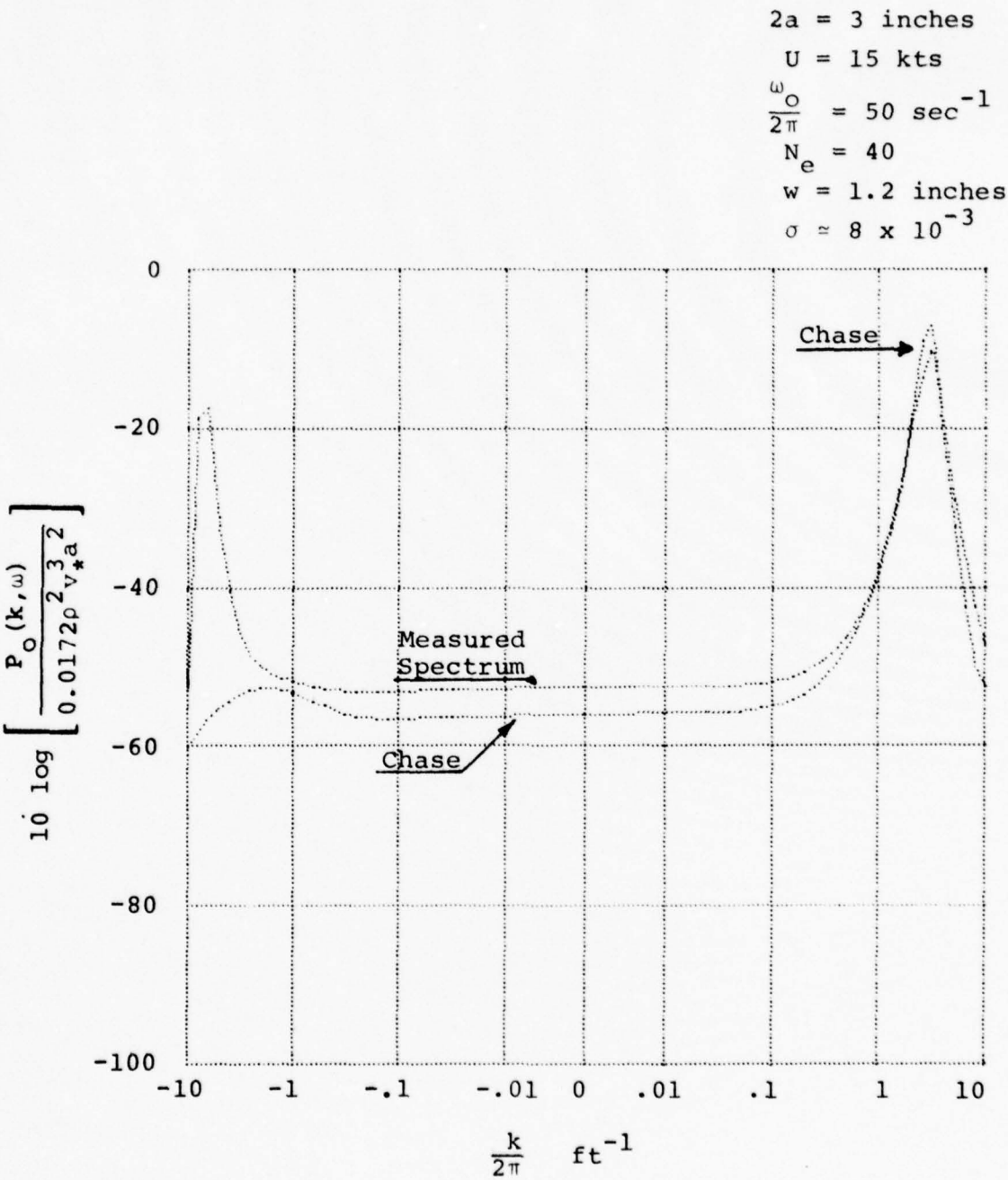

Figure 2.19. Comparison of the Measured Spectrum with the Chase Model (Large Array, Relaxed Tolerances, 50 Hz).

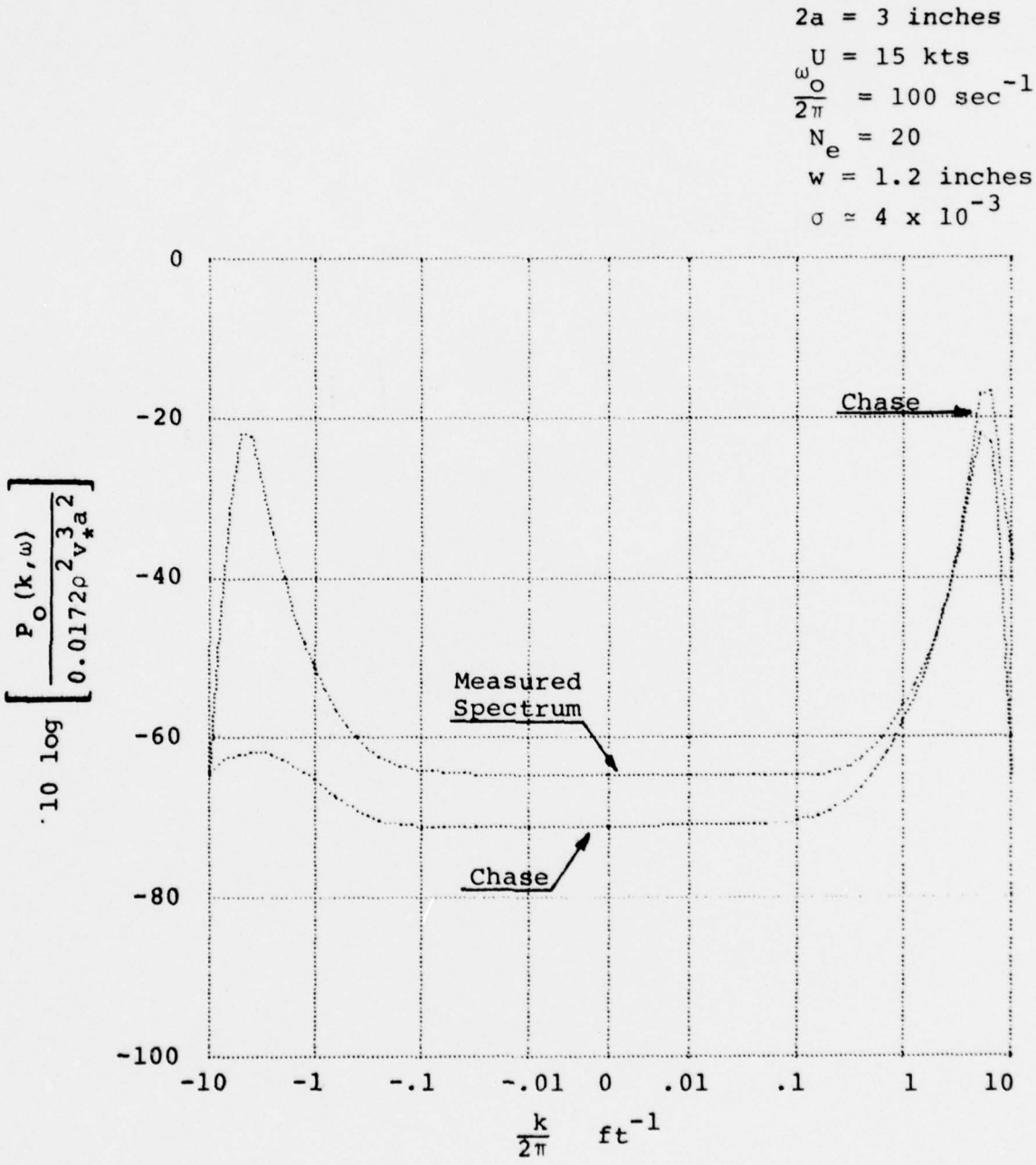

Figure 2.20. Comparison of the Measured Spectrum with the Chase Model (Small Array, Very Tight Tolerances, 100 Hz).

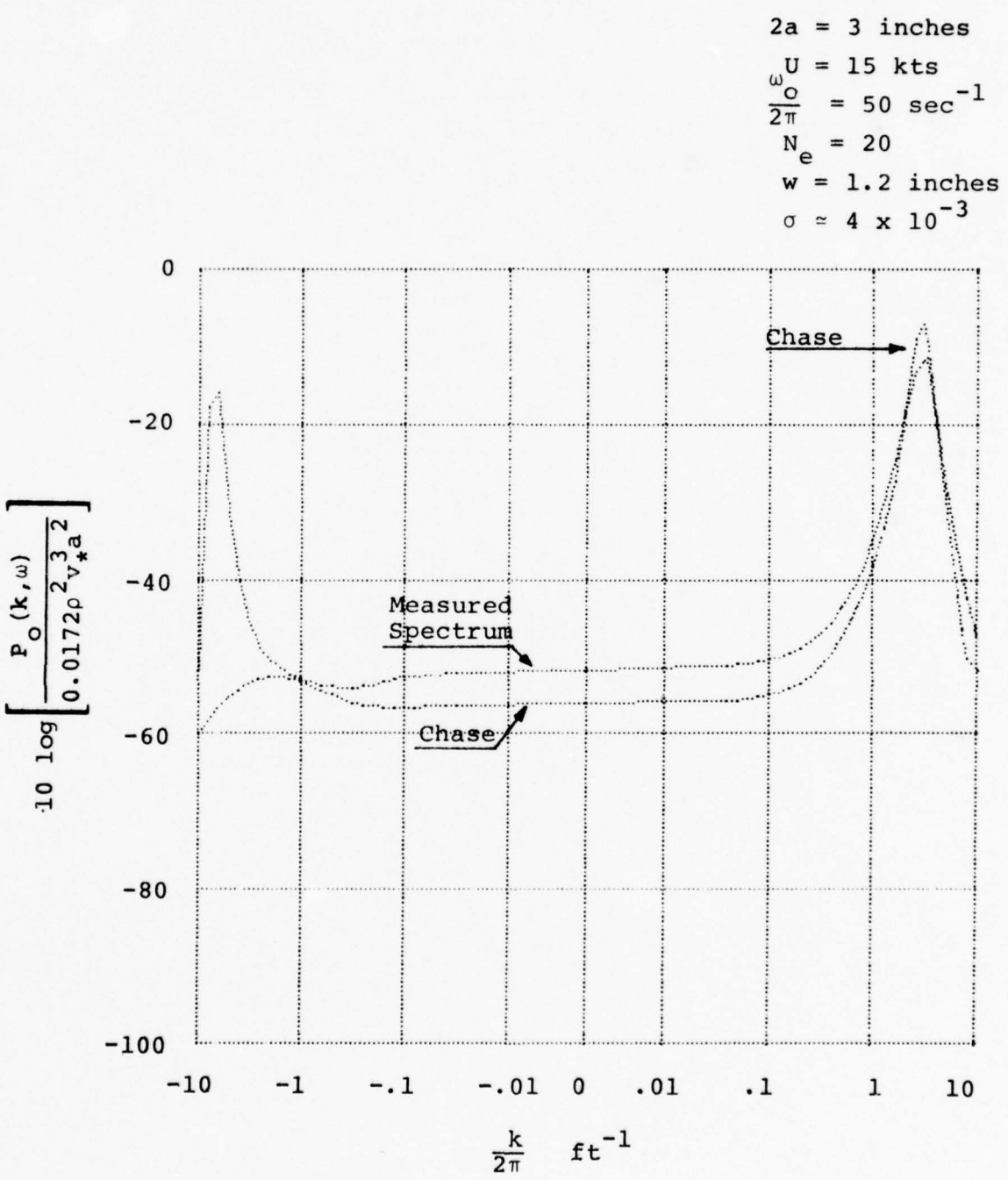

Figure 2.21. Comparison of the Measured Spectrum with the Chase Model (Small Array, Very Tight Tolerances, 50 Hz).

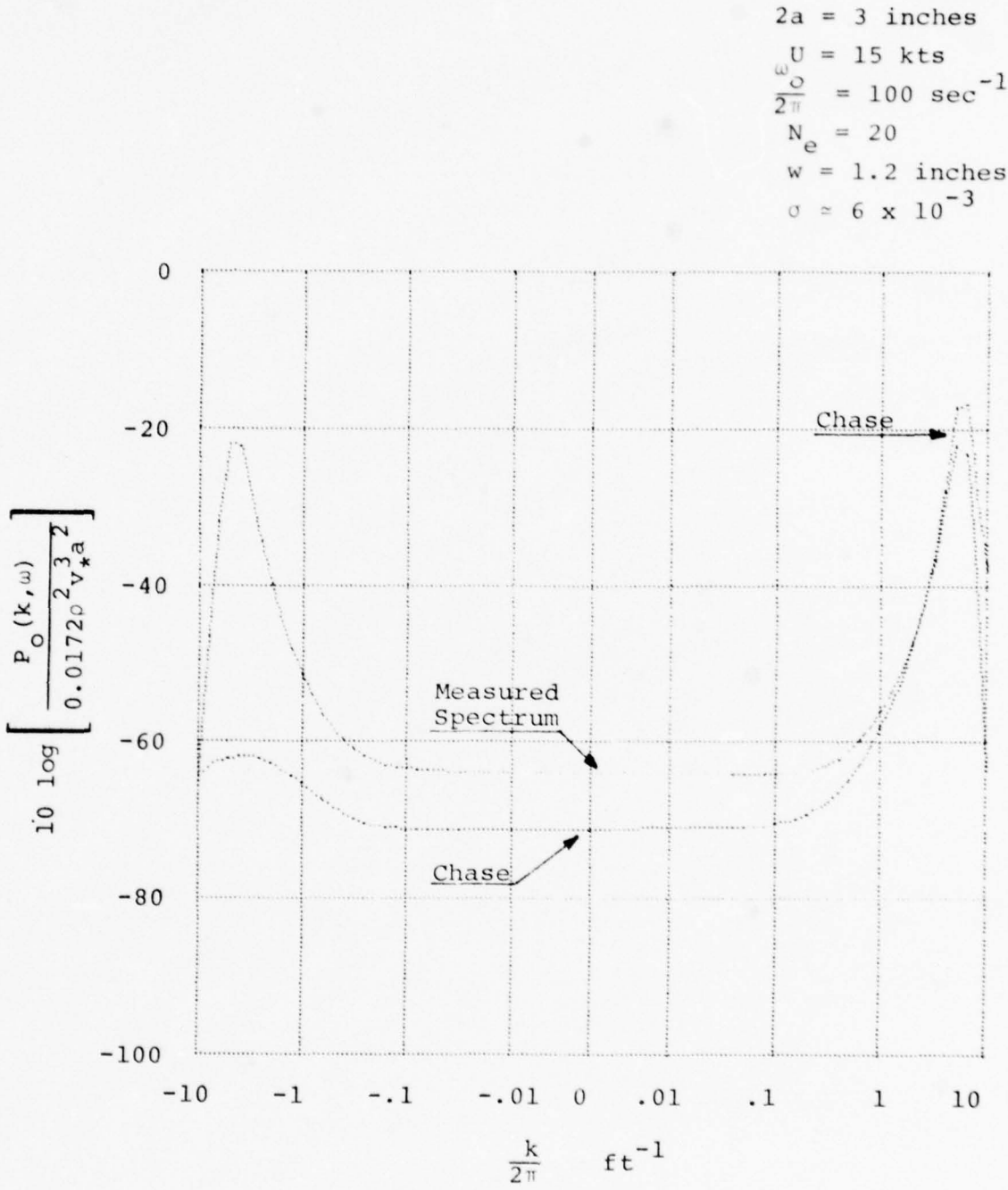

Figure 2.22. Comparison of the Measured Spectrum with the Chase Model (Small Array, Very Tight Tolerances, 100 Hz).

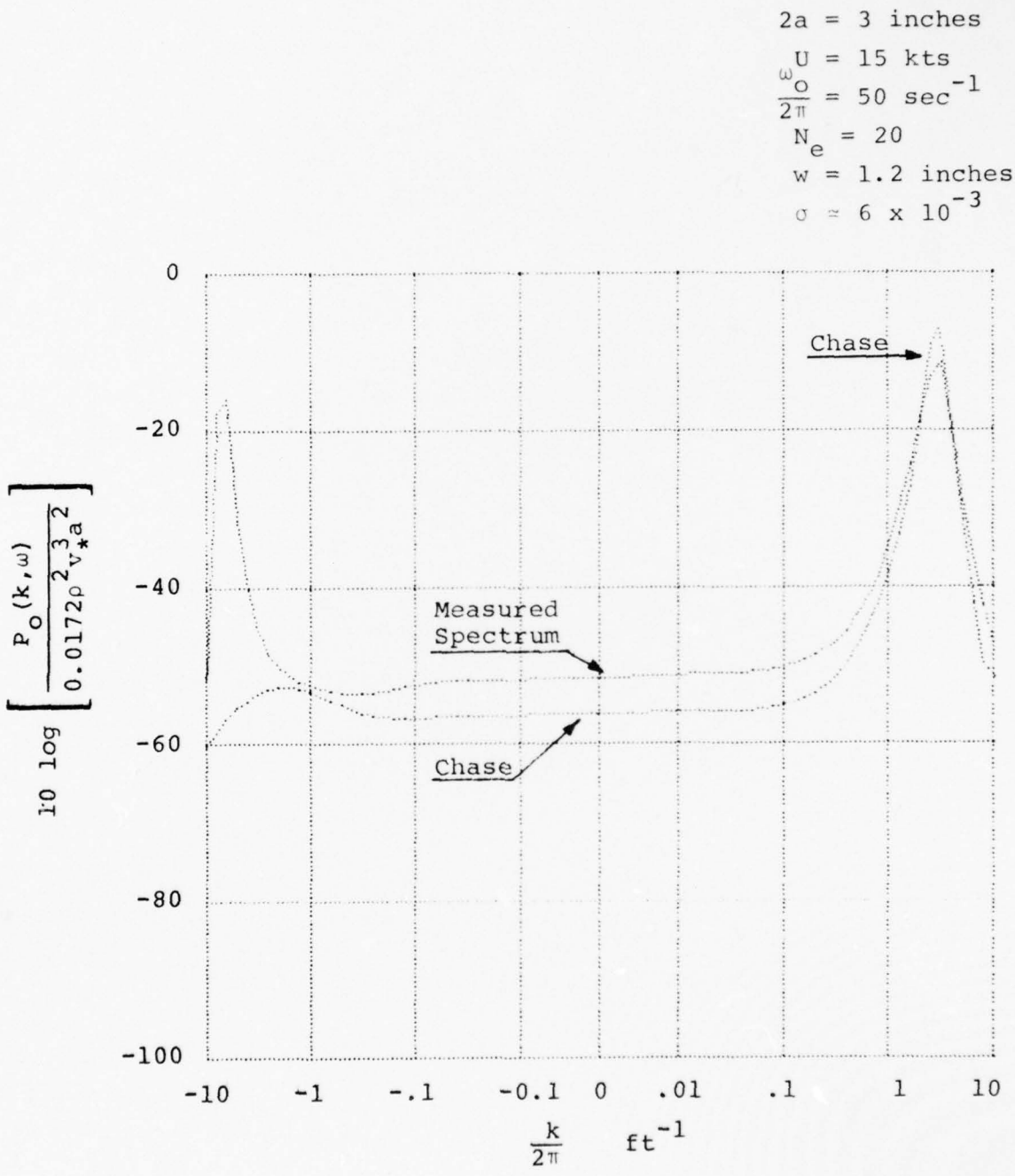

Figure 2.23. Comparison of the Measured Spectrum with the Chase Model (Small Array, Very Tight Tolerances, 50 Hz).

At 50 Hz, (Figure 2.17) the preferred array performs well. It provides a measurement within 3 dB of the Chase model over the range $-2ft^{-1} \leq (k/2\pi) \leq 4\ ft^{-1}$. This range includes the convective peak at $(k/2\pi) = 2.9ft^{-1}$. Even when the tolerances are relaxed by $\sqrt{2}$, a useful measurement range is achieved -- $0.2\ ft^{-1} \leq (k/2\pi) \leq 2\ ft^{-1}$. The measured value at the convective peak is about 4.5 dB below the Chase model. The good performance at 50 Hz can be attributed to the fact that the spectral dynamic range is 6 to 7 dB less at this frequency than at 100 Hz.

As can be seen from Figure 2.18, the performance at 100 Hz is measurably degraded by the relaxed tolerances. The bias at low wavenumber increased from 5.7 dB to 7.5 dB.

Figures 2.20 through 2.23 indicate the performance achieved by the shorter array. Due to its greater k-space bandwidth the biases have increased even though the tolerances have been decreased to maintain the same sidelobe level. The k-space region for which the bias in the measured spectrum is 3 dB or less is reduced to $.6\ ft^{-1} \leq (k/2\pi) \leq 4\ ft^{-1}$ for a center frequency of 100 Hz. The maximum bias at low wavenumber is 6.5 dB. These numbers indicate performance comparable to the 40 element array, but with greatly relaxed tolerances on the larger array. (i.e. with the tolerances on the longer array, greater by a factor of two).

At 50 Hz the shorter array performs significantly poorer than the longer array. The measurement interval has been reduced to a relatively narrow region around the convective peak. At 50 Hz, the Chase model predicts a more narrow spectrum and the wider k-space bandwidth

of the 20 element array is insufficient to reproduce it adequately.

The reduced element tolerances do not greatly further degrade the shorter array. This due, primairly, to the fact that the shorter array is already significantly limited by its k-space bandwidth.

Table 2.2 summarizes Figures 2.16 through 2.23. That table indicates why the 40 element array is preferred. At 50 Hz with the tighter tolerances it provides a very good measurement. It has the capability to reproduce the Chase model (within 3 dB) from negative wavenumbers to wavenumbers beyond the convective peak. At 100 Hz, the measurement interval is still reasonably good. The low wavenumber limit ($k/2\pi$ = .4 ft^{-1}) corresponds to wavespeeds on the order of 250 ft/sec. This limit is comparable to the breathing wavespeed for many types of hose construction; thus the measurement provides useful information. The upper limit ($(k/2\pi)$ = 4 ft^{-1}) is somewhat below the convective peak. If the tolerances are relaxed by $\sqrt{2}$ (σ_G = .082 dB, σ_ϕ = .409 deg, σ_β = 2.45 mils, SL = 51.5 dB) a useful measurement range is still achieved, particularly at the lower frequency.

The 20 element array with very tight tolerances (σ_G = .041 dB, σ_ϕ = .289 deg, σ_β = 1.73 mils) provides a moderate capability at 100 Hz, but is quite limited at 50 Hz due to its relatively wide k-space bandwidth.

2.3 Capability at other Tow Speeds and Frequencies

The last two columns of Table 2.2 indicate the Strouhal number, N_s, and normalized wavenumbers, ka, corresponding to the frequency and measurement intervals respectively. Since the Chase model, as presented in Appendix A, depends only on Strouhal number and normalized wavenumber, the prefered array should provide a good measurement capability for $N_s \lesssim 3$, and $0 < ka \lesssim .08$. (Of course if the array diameter is changed, the element size should be scaled proportionally). The above limits are reasonable engineering "guesstimates", however the scaling of the spectrum given in Appendix A should not be accepted without reservation. In particular, a dimensional analysis indicates that the spectrum should depend on other dimensionless parameters such as (v_*/U), (δ/a), etc. The model presented in Appendix A makes the implicit assumption that for typical towspeeds, array size and construction, etc. these parameters are nominally constant. This is probably incorrect, in general, but is a reasonable engineering approximation for three inch cylinders at typical tow speeds.

TABLE 2.2

SUMMARY OF TWO ARRAYS

· Element width = Element spacing = 1.2 in.

Number of Elements	Tolerances σ_G (dB)	σ_ϕ (deg.)	σ_β (mils)	RMS Sidelobe Level (dB)	Freq. $(\omega/2\pi)$ (Hz)	Measurement Interval $(k/2\pi)$ min (ft^{-1})	max (ft^{-1})	Strouhal Number $\frac{\omega a}{U}$	Normalized Meas. Interval (ka) min	max
40	.058	.289	1.73	54.5	100	+.4	+4.0	3.1	8×10^{-3}	8×10^{-2}
					50	-2.0	+4.0	1.5	-4×10^{-2}	8×10^{-2}
	.082	.409	2.45	51.5	100	+.6	+4.0	3.1	1.2×10^{-2}	8×10^{-2}
					50	+.2	+4.0	1.5	4×10^{-3}	8×10^{-2}
20	.041	.204	1.22	54.5	100	+.6	+4.0	3.1	1.2×10^{-2}	8×10^{-2}
					50	+1.6	+2.0	1.5	3.2×10^{-2}	4×10^{-2}
	.058	.289	1.73	51.5	100	+.7	+4.0	3.1	1.4×10^{-2}	8×10^{-2}
					50	+1.6	+2.0	1.5	3.2×10^{-2}	4×10^{-2}

REFERENCES

[1] L. W. Brooks, "Array Design Considerations for the Measurement of the Low-wavenumber Content of Turbulent-Boundary-Layer Wall Pressure", Report No. WB77-13, Binary Systems, Inc., Silver Spring, MD., Dec. 30, 1977.

[2] S. Gardner, "Summary of Recent Results Concerning Low-Wavenumber Boundary Layer Turbulence", Report D77-106, Contract N00014-72-C-0318, Binary Systems, Inc. 88 Sunnyside Blvd, Plainview, New York, 11803, Jan 10, 1977.

[3] D. M. Chase, "Modeling of Turbulent Wall-Pressure Spectra on Towed Cylinders", Technical Memo 352, Contract No. N66001-77-C-0114, Bolt, Beranek and Newman, Inc., 50 Moulton Street, Cambridge, MASS., 02138, May 23, 1977.

[4] W. W. Willmarth, R. E. Winkel, L. K. Sharma, and T. J. Bogar, "Axially Symmetric Turbulent Boundary Layers on Cylinders: Mean Velocity Profiles and Wall Pressure Fluctuations", J. Fluid Mech., (1976) Vol 76, Part 1, pp 35-64.

[5] W. W. Willmarth and C. S. Yang, "Wall-Pressure Fluctuations beneath Turbulent Boundary Layers on a Flat Plate and a Cylinder", J. Fluid Mech. (1970) Vol. 41, part 1, pp 47-80.

[6] A. E. Markowitz, " Turbulent Boundary Layer Wall Pressure Fluctuation and Wall Acceleration Measurements on a Long Flexible Wall Cylinder Towed at Sea", NUSC Tech. Report 5305, Naval Underwater Systems Center, New London, Conn., 12 Aug, 1976.

[7] F. Harris, "On the Use of Windows for Harmonic Analysis with the Discrete Fourier Transform", Proc. IEEE, Vol 66, No. 1, Jan., 1978, pp 51-83.

[8] H. Urkowitz, J. Geisler, and N. Riccardi, "The Effect of Weighting upon Signal-to-Noise Ratio in Pulse Bursts", IEEE Trans., Vol. AES-9, July 1973, pp 486-494.

APPENDIX A: SPECTRAL NOTATION

Let $p(\zeta,\theta,\tau)$ denote the pressure fluctuations on the surface of the cylinder at distance ζ along the cylinder, angle θ around the cylinder and time τ. The pressure is assumed to be stationary in all three coordinates so that the origin of the coordinate system is not important. Let $W(\zeta,\theta,\tau)$ denote the space-time correlation function:

$$W(\zeta,\theta,\tau) = E(p(\zeta_1,\theta_1,\tau_1)P(\zeta_1+\zeta,\theta_1+\theta,\tau_1+\tau)) \qquad (A-1)$$

where "E" denotes statistical expectation. Since W is periodic in θ with period 2π, it has a mixed Fourier-transform Fourier-series representation:

$$W(\zeta,\theta,\tau) = \sum_{m=-\infty}^{\infty} \int_{-\infty}^{\infty} dk \int_{-\infty}^{\infty} d\omega e^{i(k\zeta+m\theta-\omega\tau)} P_m(k,\omega) \qquad (A-2)$$

with the reciprocal relation:

$$P_m(k,\omega) = (2\pi)^{-3} \int_0^{2\pi} d\theta \int_{-\infty}^{\infty} d\zeta \int_{-\infty}^{\infty} d\tau e^{-i(k\zeta+m\theta-\omega\tau)} W(\zeta,\theta,\tau) \qquad (A-3)$$

In the above relations, $P_m(k,\omega)$ is the m^{th} angular harmonic spectral density in streamwise wavenumber and frequency. The total mean square pressure fluctuation is given by:

$$E\left[p^2(\zeta,\theta,\tau)\right] = \sum_{m=-\infty}^{\infty} \int_{-\infty}^{\infty} dk \int_{-\infty}^{\infty} d\omega P_m(k,\omega)$$
$$= W(0,0,0) \qquad \text{(A-4)}$$

The quantity $P_o(k,\omega)$ is the wavenumber frequency spectrum of the axisymmetric component of pressure.

Here the narrowband coherence function is defined as:

$$\Gamma(\zeta,\theta,\omega) = \frac{1}{2\pi} \int_{-\infty}^{\infty} d\tau W(\zeta,\theta,\theta) e^{i\omega\tau} \qquad \text{(A-5)}$$

and therefore is related to the angular-harmonic spectral densities by:

$$P_m(k,\omega) = \frac{1}{(2\pi)^2} \int_0^{2\pi} d\theta \int_{-\infty}^{\infty} d\zeta \Gamma(\zeta,\theta,\omega) e^{-(k\zeta+m\theta)} \qquad \text{(A-6)}$$

In this notation, the frequency spectral density of the directly transmitted TBL pressure in the center of a fluid filled hose is given approximately by:

$$P_T(\omega) \simeq \int_{-\infty}^{\infty} dk P_o(k,\omega) |G_o(k)|^2 \qquad \text{(A-7)}$$

where $G_o(k)$ is the hose transfer function from axisymmetric pressure to internal pressure. For a lightly damped hose, with a breathing speed much greater than the convection

velocity. This is approximated as:

$$P_T(\omega) \approx \left(\frac{\pi\omega}{2c_o\zeta}\right)\left[P_o\left(\frac{\omega}{c_o},\omega\right) + P_o\left(\frac{-\omega}{c_o},\omega\right)\right] \qquad \text{(A-8)}$$

where c_o is the breathing wavespeed and ζ is the hose damping factor. The one-sided spectral level (per Hz) is given as:

$$L_T(\omega) = 10 \log [4\pi P_T(\omega)] \qquad \text{(A-9)}$$

Chase [2] gives the following expression for P_o:

$$P_o(k,\omega) = \frac{c_t \rho^2 v_*^3}{a} K^2 K_t^{-5} \qquad \text{(A-10)}$$

$$c_t = 0.063$$
$$v_* = .04U$$
$$K^2 = k^2 + \frac{1}{12a^2}$$
$$K_t^2 = \left(\frac{\omega - U_c k}{h v_*}\right)^2 + \frac{1}{\Delta^2} + k^2$$
$$U_c = 0.68U$$
$$\Delta = 1.08a$$
$$h = 3.7$$

In general, the various dimensionless parameters, c_t, (v_*/U), (Δ/a), h, (U_c/U), etc. are thought to depend on (δ/a), where δ is the boundary layer thickness. The

ratio (δ/a), in turn, will depend on downstream location. However, Chase does not give functional relations for these parameters. Here they are assumed to be constant over the applicable range of tow speeds and streamwise position. With this very crude assumption, one may write:

$$P_o(k,\omega) = c_t \rho^2 v_*^3 a^2 (Ka)^2 (K_t a)^{-5} \qquad \text{(A-11)}$$

and

$$(Ka)^2 = (ka)^2 + \frac{1}{12}$$

$$(K_t a)^2 = \left(\left(\frac{\omega a}{U}\right)\left(\frac{U}{hv_*}\right) - \left(\frac{U_c}{hv_*}\right)(ka)\right)^2 + (ka)^2 + .85$$

and the spectrum scales according to the Strouhal number $N_s = (\omega a/U)$ and normalized wavenumber, ka.

Gardner [3] used a different normalization in developing his model for P_o. If this author has correctly interpreted the normalization used by Gardner, his model may be written:

$$P_o(k,\omega) = \frac{\phi(\omega)}{8\pi^2}\left[\frac{1-e^{-\pi\alpha_2 N_s}}{\pi\alpha_2 N_s}\right] G \qquad \text{(A-12)}$$

where

$$G = \frac{2\alpha_1 N_s}{\left(\alpha_1 N_s \frac{U}{U_c}\right)^2 + \left(ka - \frac{U}{U_c} N_s\right)^2}$$

and

$$\phi(\omega) = \frac{2\rho^2 v_*^3}{N_s^2}\left(\frac{v^*}{U}\right)a^2$$

In the above expression N_s is the Strouhal number ($\omega a/U$), and α_1 and α_2 are constants given by -- $\alpha_1 = 0.1$, $\alpha_2 = 1.7$. Again making the crude assumption that α_1, α_2, (v^*/U), and U_c/U are constant, the Gardner model also scales according to N_s and ka.

As a check on the normalization, it is noted that Equation (A-9) agrees with that given by Gardner [3] for the directly transmitted TBL pressure.

For purposes of scaling, the plots presented earlier, were normalized by the maximum over frequency and wavenumber of the Chase model. This maximum is given approximately by:

$$P_{max} = \max_{-\infty \le k \le \infty} \max_{-\infty \le \omega \le \infty} P_o(k,\omega)$$

$$\simeq 0.0172\rho^2 v_*^3 a^2 \qquad \text{(A-13)}$$

APPENDIX B: THE EFFECT OF AMPLITUDE, PHASE AND POSITION ERRORS ON THE ARRAY FACTOR

The array response to wavenumber, k when steered to wavenumber k_s can be written as:

$$B(k,k_s) = \sum_{\ell=1}^{N_e} V_\ell e^{ik[(\ell-1)d+\beta_\ell]} \qquad \text{(B-1)}$$

where

β_ℓ is the position error of the ℓ^{th} element.

Now from Equation 2.1:

$$V_\ell = a_\ell e^{-ik(\ell-1)d} \qquad \text{(B-2)}$$

so that

$$B(k,k_s) = \sum_{\ell=1}^{N_e} a_\ell e^{i[(k-k_s)(\ell-1)d + k\beta_\ell]} \qquad \text{(B-3)}$$

Note that B cannot be written as a function only of the difference $k-k_s$.

Now if amplitude and phase errors are present, a_ℓ can be written:

$$a_\ell = a_\ell^o(1+\varepsilon_\ell)e^{i\phi_\ell} \qquad \text{(B-4)}$$

where

a_ℓ^o is the true (error free) amplitude,

ε_ℓ is the fractional amplitude error

and

ϕ_ℓ is the phase error.

Substituting (B-4) into (B-3), and squaring the magnitude yields:

$$|B(k,k_s)|^2 = \sum_{\ell,m} a_\ell^o a_m^o e^{j(k-k_s)(\ell-m)d}(1+\varepsilon_\ell)(1+\varepsilon_m)e^{j(\psi_\ell-\psi_m)} \tag{B-5}$$

where ψ_ℓ is given by:

$$\psi_\ell = \phi_\ell + k\beta_\ell \tag{B-6}$$

Assuming zero mean errors, independence between amplitude, phase and position errors, independence between channels and small errors yields:

$$E(1+\varepsilon_\ell)(1+\varepsilon_m)e^{j(\psi_\ell-\psi_m)} = E[(1+\varepsilon_\ell)(1+\varepsilon_m)]Ee^{j(\psi_\ell-\psi_m)}$$

$$\simeq (1+\delta_{\ell m}\sigma_\varepsilon^2)\ E[1 + j(\psi_\ell-\psi_m) + j^2(\psi_\ell-\psi_m)^2/2]$$

$$= (1+\delta_{\ell m}\sigma_\varepsilon^2)(1-(1-\delta_{\ell m})\sigma_\psi^2)$$

$$\simeq 1 + \delta_{\ell m}\sigma_\varepsilon^2 - (1-\delta_{\ell m})\sigma_\psi^2 \tag{B-7}$$

Thus the expected value of the magnitude of the array response is given by:

$$E|B(k,k_s)|^2 = \sum_{\ell,m} a_\ell^o a_m^o e^{ik(\ell-m)d} + \sigma_\varepsilon^2 \sum_\ell (a_\ell^o)^2 - \sigma_\psi^2 \sum_{\ell \neq m} a_\ell^o a_m^o e^{ik(\ell-m)d}$$

$$= |A(k-k_s)|^2 (1-\sigma_\phi^2 k^2 \sigma_\beta^2) + (\sigma_\varepsilon^2+\sigma_\phi^2+k^2\sigma_\beta^2) \sum_\ell (a_\ell^o)^2 \qquad \text{(B-8)}$$

Recall that the white noise loss factor is given by:

$$\ell_W = \frac{N_e \sum_\ell (a_\ell^o)^2}{(\sum_\ell a_\ell^o)^2} = N_e \sum (a_\ell^o)^2 \qquad \text{(B-9)}$$

since it has been assumed that

$$A(0) = \sum_\ell a_\ell^o = 1 \qquad \text{(B-10)}$$

Thus the average power response can be written:

$$E|B(k,k_s)|^2 = |A(k-k_s)|^2 (1-\sigma_\phi^2 - k^2\sigma_\beta^2) + (\sigma_\varepsilon^2+\sigma_\phi^2+k^2\sigma_\beta^2) \frac{\ell_W}{N_e} \qquad \text{(B-11)}$$

LIST OF SYMBOLS

a	cylinder radius
a_ℓ	weighting coefficient chosen to control the sidelobe response of the array
a_ℓ^o	errorless weighting coefficient
$A(k)$	"array factor" (Eq. 2.3)
B	k-space bandwidth near the convective peak
$B(k,k_s)$	array response at wavenumber k when steered to wavenumber k_s
c	acoustic propagation velocity
c_o	breathing (bulge) wavespeed
c_t	dimensionless constant in the Chase model of $P_o(k,\omega)$
d	separation between elements
DR	spectral dynamic range (in dB)
$E(\cdot)$	statistical expectation operator
f	reciprocal period (frequency)
$G_o(k)$	hose transfer function from axisymmetric pressure to internal pressure
$H(k)$	element factor representing the response of a single element to wavenumber, k
k	wavenumber (2π times reciprocal wave length)
k_B	k-space 3 dB bandwidth of the array factor
k_c	wavenumber at convective peak ($k_c = \omega/U_c$)
k_s	wavenumber to which the array is steered (Eq. 2.1)
ℓ_W	white noise loss factor (Eq. 2.4)
L_T	one sided spectrum level of the directly transmitted TBL pressure (Eq. A-9)
N_e	number of array elements
N_s	Strouhal number, ($\omega a/U$)

$p(\zeta,\theta, t)$	point pressure
P_A	aliased spectrum (Eq. 2.5)
P_M	measured wavenumber-frequency spectrum
$P_o(k,\omega)$	wavenumber-frequency spectrum for the axisymmetric component of wall pressure
$P_T(\omega)$	frequency spectral density of the directly TBL pressure (Eq. A-7)
$Q(\omega)$	measured frequency spectral density of the point surface pressure under a TBL
SL	array sidelobe level (in dB)
U	free stream speed
U_c	convection velocity
$v_\star$	shear velocity
V_ℓ	complex multiplier applied to the ℓ^{th} element (Eq. 2.1)
w	element width
$W(\zeta,\theta,\tau)$	autocorrelation function of the point surface pressure under the TBL
δ	Dirac delta function
Δ	see Eq. A-10
ΔG	channel gain deviation
$\Delta\beta$	hydrophone position deviation
$\Delta\Phi$	channel phase deviation
ε_ℓ	fractional amplitude error on the ℓ^{th} element
ρ	fluid density
σ	reciprocal wavelength
σ_G	rms channel-to-channel gain tolerances
σ_k	k-space rms bandwidth (Eq 2.7)
σ_β	rms channel-to-channel position tolerances
σ_ε	rms channel-to-channel fractional amplitude
σ_ϕ	rms channel-to-channel phase tolerance
ω	frequency (2π times reciprocal period)

ONR DISTRIBUTION LIST

	Number of Copies
Defense Documentation Center Cameron Station Alexandria, Virginia 22314	12
Director Naval Research Laboratory Code 2627 4555 Overlook Avenue S. W. Washington, D. C. 20375	6
Office of Naval Research Branch Office 495 Summer Street Boston, Mass. 02210	
Office of Naval Research Branch Office 536 South Clark Street Chicago, Illinois 60605	
Office of Naval Research Branch Office 1030 East Green Street Pasadena, California 91106	
Commander Naval Sea Systems Command Department of the Navy Washington, D. C. 20362 Code 06H1	C. Walker
Commander Naval Sea Systems Command Department of the Navy Washington, D. C. 20362 Code 06H2	
Commander Naval Electronic Systems Command Code 320 2511 Jefferson Davis Highway National Center #1 Arlington, Virginia 20360	
Commander Naval Electronic Systems Command PME 124-40 2511 Jefferson Davis Highway National Center #1 Arlington, Virginia 20360	

Commanding Officer
Naval Underwater Systems Center
Central Test & Evaluation Activity
1651 SW 40th Street
Fort Lauderdale, Florida 33315

Commanding Officer
Naval Ocean Research & Development Activity
NSTL Station
Bay St. Louis, Mississippi 39529

Chief of Naval Material
NAVMAT 03T
Arlington, Virginia 20360

Commander
Naval Ocean Systems Center
San Diego, California 92152

Commander
David W. Taylor Naval Ship Research
& Development Center
Bethesda, Maryland 20084

Dr. P. Rispin

C. Campbell
Arthur D. Little, Inc.
Acorn Park
Cambridge, Mass. 02140

Binary Systems, Inc.
88 Sunnyside Blvd
Plainview, New York 11803

Johns Hopkins University
Applied Physics Laboratory
SSBN Security Program
Johns Hopkins Road
Laurel, Maryland 20810

A. M. Chwastyk

EDO Corporation
1310 11th Street
College Point, New York 11356

J. Schere

General Dynamics Corporation
Electric Boat Division
Eastern Point Road
Groton, Connecticut 06340

Project Manager Anti-Submarine Warfare Systems Project (PM-4) Department of the Navy Washington, D. C. 20362	Capt R.E. Adler,ASW-13
Office of Naval Research 800 N. Quincy Street Arlington, Virginia 22217	Code 212 H. Fitzpatrick Code 222 G. Boyer
Commander Naval Undersea Center San Diego, California 92132	Dr. R. Smith R. Koelsar
Commanding Officer Naval Underwater Systems Center New London Laboratory New London, Conn. 06320	Dr. H. Schloemer Dr. W. Strawderman R. Kennedy A. Markowitz E. Racine
Bolt Beranek & Newman, Inc. 50 Moulton Street Cambridge, Mass. 02138	Dr. D. Chase Dr. K. Chandiramani
Hughes Aircraft Company Ground Systems Group 1901 West Malvern Avenue Fullerton, Calif. 92634	D. Veronda
Sperry Gyroscope Information and Communication Div. Great Neck, New York 11020	G. Rand
General Electric Company Heavy Military Electronic Systems Syracuse, N. Y. 13201	Don Braite
Ratheon Corporation Submarine Signal Division Portsmoutn, RI 02871	Phil Brooks
Bolt Beranek & Newman, Inc. 1701 North For Myer Drive Arlington, Virginia 22209	
Gould Incorporated Chesapeake Instrument Division 6711 Baymeadow Drive Glen Burnie, Md. 21061	

Professor Patrick Leehey
Room 5-222
Massachusetts Institute of Technology
Acoustics and Vibration Laboratory
70 Massachusetts Avenue
Cambridge, Mass. 02139

Professor W. W. Willmarth
The University of Michigan
Aerospace Engineering, North Campus
Ann Arbor, Michigan 48109

Binary Systems, Inc.
10750 Columbia Pike
Silver Spring, Md. 20901

F. Rees

MAR, Inc.
1335 Rockville Pike
Rockville, Maryland 20852

REPORT DOCUMENTATION PAGE

READ INSTRUCTIONS BEFORE COMPLETING FORM

1. REPORT NUMBER: CBR-79-01	2. GOVT ACCESSION NO.
3. RECIPIENT'S CATALOG NUMBER	
4. TITLE (and Subtitle): FURTHER RESULTS ON AN ARRAY DESIGN TO MEASURE THE WAVENUMBER-FREQUENCY SPECTRUM BENEATH AN AXISYMMETRIC TURBULENT BOUNDARY LAYER	5. TYPE OF REPORT & PERIOD COVERED: Final
	6. PERFORMING ORG. REPORT NUMBER: ------
7. AUTHOR(s): Dr. L. W. Brooks	8. CONTRACT OR GRANT NUMBER(s): ONR - N00014-72-C-0318
9. PERFORMING ORGANIZATION NAME AND ADDRESS: Binary Systems, Inc. 303 E Street, P.O. Box 1105 Salida, Colo. 81201	10. PROGRAM ELEMENT, PROJECT, TASK AREA & WORK UNIT NUMBERS: ------
11. CONTROLLING OFFICE NAME AND ADDRESS: Office of Naval Research, Code 222 800 N. Quincy Street Arlington, Virginia 22217	12. REPORT DATE: Feb. 5, 1979
	13. NUMBER OF PAGES: 70
14. MONITORING AGENCY NAME & ADDRESS (if different from Controlling Office): N/A	15. SECURITY CLASS. (of this report): Unclassified
	15a. DECLASSIFICATION/DOWNGRADING SCHEDULE

16. DISTRIBUTION STATEMENT (of this Report)

Unlimited

DISTRIBUTION STATEMENT A
Approved for public release;
Distribution Unlimited

17. DISTRIBUTION STATEMENT (of the abstract entered in Block 20, if different from Report)

18. SUPPLEMENTARY NOTES

19. KEY WORDS (Continue on reverse side if necessary and identify by block number)

LOW WAVENUMBER SPECTRUM
AXISSYMMETRIC TURBULENT BOUNDARY LAYER
WAVE VECTOR FILTERING

20. ABSTRACT (Continue on reverse side if necessary and identify by block number)

This report describes the requirements on a flush mounted array designed to measure the wavenumber-frequency spectrum of the axisymmetric component of wall pressure beneath an axially towed cylinder. Measurement of the low wavenumber content is emphasized. The effect of the wavenumber spectral dynamic range as well as channel-to-channel amplitude, phase and position tolerances are evaluated.

DD FORM 1 JAN 73 1473 EDITION OF 1 NOV 65 IS OBSOLETE
S/N 0102-LF-014-6601

SECURITY CLASSIFICATION OF THIS PAGE (When Data Entered)